Studies on Photo-initiation of Nanostructure Materials by Femtosecond Laser Irradiation

Wu Nan

2012

Content

General Introduction…….1

Chapter 1

Formation of micro-structuring with femtosecond laser…….11

Chapter 2

Selective metallization of Ag_2O-doped silicate glass by femtosecond laser direct writing……...30

Chapter 3

Nano-periodic structure formation on titanium thin film with a femtosecond laser……52

Chapter 4

Photo-initiation of ZnO nanowire formation by femtosecond laser irradiation…….68

Summary……98

List of Publications

Acknowledgement

General Introduction

The ultrafast laser has been used as a powerful tool to clarity elementary processes, such as excitation-energy relaxation and both electron and proton transfer on nanosecond and picoseconds time scales that occur in a micrometer-sized area. In the past decades, the ultrafast laser has been widely used in micro processing. A femtosecond laser, which is the typical ultrafast laser, has two apparent features: (1) elimination of the thermal effect due to extremely short energy deposition time, and (2) participation of various nonlinear processes enabled by strong localization of laser photons in both time and spatial domains. Due to the ultrashort light-matter interaction time and the high peak power density, material processing with the femtosecond laser is generally characterized by the absence of heat diffusion and consequently molted layers. The photo-induced reactions are expected to occur only near the focused part of the laser beam due to multiphoton processes. Therefore, much attention has been paid to manufacture micromachine by using femtosecond laser irradiation, such as micro-total-analysis-system [1-4] and lab-on-a-chip (LOC) devices due to their highly efficient operation, allowing chemical reactions and biomedical analysis to be performed with minute amounts of samples [5–8]. In these devices, micromechanical components such as micropumps, microvalves and micromixers are integrated with microfluidics in a single glass chip with a size of the order from mm^2 to tens of cm^2 for allow metering dilution, flow switching, particle separation, mixing, pumping, the incubation of reaction materials and reagents, and sample dispensing or injection.

The most common methods of microstructure processing include chemical processing,

energy beam processing, composite processing and scanning probe processing. However, glass-like substance is hard and brittle, micro-machining is difficult. One preparation strategy for μ-TAS devices [9-11] is to use vacuum evaporation [12] or chemical vapor deposition (CVD) [13] to deposit metal thin films on a glass chip, but these methods are complicated and onerous in view of a needed resist process and vacuum for photolithography in micropatterning. So a simple processing method must be seeking. Laser direct writing is expected to be an alternative method to forming patterns of microstructure on the surface of materials without photolithography.

Not only the femtosecond laser has been widely applied to micrometer-sized area, but also in the field of nanotechnology it can also be widely used. The laser-induced ablation method has become an increasingly popular approach for making nanopartcles from the viewpoint of the concise procedure and application of a variety of materials [14,15]. The ripple structures have been observed on the surface of the metal and semiconductor cause by the interferences between the scattering incident laser field and the surface Plasmon-polariton waves (SPWs) [16]. And Y. Shimotsuma et al. have reported the observation of the photoconversion from copper flakes to nanowires even nanospheres formation via ultrafast pulse laser irradiation in ethanol.

In this work, a femtosecond laser is used for photo-initiation of micro-structuring (micro-size or nano-size) on the Inorganic materials and is investigated the dependence between formation and mechanism. Femtosecond laser is one of the pulsed laser that emits ultrashort optical pulses that have a pulse width with femtosecond (10^{-15} second) range. Femtosecond laser is superior to modify an irradiation area of materials as

compared to other pulse lasers having pulse duration beyond one picosecond. First, since the pulses is compressed and emitted for ultrashort time, it is possible to gain large peak intensity with same pulse. Second, tightly focused femtosecond laser can induce nonlinear absorption of light in transparent material leading to change of material properties at the focal volume. Third, short pulses require less energy than longer pulses to reach the threshold for optical breakdown. Decreasing the photon energy leads to more precise processing or material modification.

Damage mechanism using femtosecond laser pulses is fundamentally different from that of another such as picosecond or nanosecond laser. The laser wavelengths of pulse lasers having a pulse width of nanosecond or longer duration are usually in the ultraviolet regions, therefore, interactions between light - materials occur at the surface of the material. For pulse durations longer than a few tens of picoseconds, the energy is transferred from the laser-excited electrons to the lattice on the time scale of the pulse duration. This energy is then carried out of the focal volume by thermal diffusion. Damage occurs when the temperature of the material in the irradiated region reaches high enough for the material to melt or fracture [17].

On the other hand, when a femtosecond laser pulse with high peak intensity is focused into a microscopic area of transparent material, nonlinear photoionization occurs at the focal point [18,19]. Photoionization refers to direct excitation of the electron by the laser field. There are two schemes of photoionization, the multiphoton ionization and the tunneling ionization depending on the frequency and intensity of the laser. For strong laser fields and low laser frequency, the tunneling ionization is

dominant; the Coulomb well is suppressed enough that a valence electron tunnels through the barrier and becomes free. At high laser frequencies, multi-photon absorption occurs which indicates that an electron absorbs several photons simultaneously. A single photon of visible light does not have enough energy to excite an electron in a transparent material from the valence to the conduction band. However, the electron can be promoted from the valence to the conduction band when the number of photons absorbed time the photon energy is equal to or greater than the band-gap of the material, even though the wavelength of excitation does not agree with that of absorption region of the material. Once a free electron in the conduction band is produced, it become a "seed" electron that can absorb photons through inverse Bremsstrahlung absorption and gain energy during the process. After a sequence of several inverse Bremsstrahlung absorption processes, the kinetic energy is sufficiently large to collisionally ionize another electron from the valence band [19-21]. Then, two electrons are ready to gain energy through inverse Bremsstrahlung absorption, and the repeating sequence of the inverse Bremsstrahlung absorption and collisional ionization results in an avalanche growth in the number of free electrons. This process is called "avalanche ionization" [22]. Because, a time scale of photon absorption by an electron is shorter than that of energy transfer to the lattice and lattice heating processes, free electrons promoted from valence to the conduction band by the nonlinear excitation are further heated by the laser pulse much faster rather than the speed they can cool by phonon emission. The density of the nonlinearly excited electrons grows through avalanche ionization until the excited electrons gain enough energy to excite other

bound electrons. When the excited electrons acquire the critical density, they behave as plasma having the resonant frequency of the incident laser. Because the presence of plasma results in a decrease in the refractive index, most of the laser energy is absorbed [23,24]. After the laser pulse is gone, the energy is transferred from the electrons to the lattice. A short time scale of energy deposition suppresses heat diffusion out of the focal point area. As a result of the tight focusing and nonlinear absorption process, a phase or structural modification occurs only in selective internal area, resulting in permanent change in the properties of materials without surface damages [25-29]. Depending on the laser irradiation condition, cracking, pore formation or localized melting occurs. Furthermore, the modified area after laser irradiation often shows a permanent change in a size range down to the nanometer, which is smaller than the laser wavelength. For example, there are several reports on the capabilities for the subwavelength processing of femtosecond laser involving the alignment of periodic nanometer-scale grating in glass, cross patterning based on local dislocations, and the formation of nano-rods on silicon [30-32].

In this research, femtosecond laser is utilized for micro-structure of different materials. First, a new method had been developed that can selectively plate with drawing directly on the surface of Ag_2O-doped silicate glass using a femtosecond laser. It is mean that the Copper can be plated selectively. Then, a study of nano-structrues of various periodic on the film surface was investigated. One-dimensional periodic structure as nano-ripple or nano-grating had been formed. Also, not just one-dimension, a two-dimensional nanostructure as nano-net was also produced by femtosecond laser

irradiation. In addition, not just investigate light-matter interaction of the solid, our studies are also expanded to light- liquid interaction. The synthesis of ZnO nanorods can be control, and it was found that the ZnO nanotods fabricated by laser irradiation and heat treatment are smaller than those due to heat treatment only. In addition, ZnO nanostructures can be controlled by the PH of the solution. The development of high performance devices such as UV-sensor, gas sensor can be expected.

Chapter 1: The concept of femtosecond laser, a new regime of light – matter interactions are reviewed. The current state and future perspective of the femtosecond laser applications and efforts in the development of new materials are described.

Chapter 2: In this chapter, I had investigated the selective metallization on Ag_2O-doped silicate glass under femtosecond laser irradiation after electroless plating. And demonstrate the microstructures formation and discuss the mechanism and possible applications of the observed phenomena by the femsecond laser irradiation.

Chapter 3: In this chapter, periodic nanostructures oriented to the direction parallel to the laser polarization were manufactured on the Ti thin film surface after irradiation with a focused beam of femtosecond Ti: sapphire laser. Then according to the different irradiation technique, nanoripple and nanonet can be produce.

Chapter 4: In this chapter, it had been investigated that a photo-initiated process via femtosecond pulse-induced heterogeneous nucleation in zinc ammine complex ($Zn(NH_3)_4^{2+}$) based aqueous solution without catalyst and surfactant, followed by hydrothermal treatments for crystal growth into zinc oxide (ZnO) nanorods. The products are characterized by X-ray diffraction (XRD) and scanning electron

microscopy (SEM). And room temperature photoluminescence spectrum was obtained via aHoriba Jobin Yvon FluoroMax-P spectrometer with a Xenon lamp excitation source.

References

[1] M. Masuda, K. Sugioka, Y. Cheng, N. Aoki, M. Kawachi, K. Shihoyama, K. Toyoda, H. Helvajian, and K. Midorikawa, Appl. Phys. A: Mater. Sci. Process. 76 (2003) 857.

[2] Y. Cheng, K. Sugioka, K. Midorikawa, M. Masuda, K. Toyoda, M. Kawachi, and K. Shihoyama, Opt. Lett. 28 (2003) 1144 .

[3] M. Masuda, K. Sugioka, Y. Cheng, T. Hongo, K. Shihoyama, K. Toyoda, H. Takai, I. Miyamoto, and K. Midorikawa, Appl. Phys. A: Mater. Sci. Process. 78 (2004) 1029

[4] Y. Cheng, K. Sugioka, and K. Midorikawa, Opt. Lett. 29 (2004) 2007.

[5] K. Sugioka, Y. Cheng and K. Midorikawa, Appl. Phys. A **81** (2005) 1.

[6] K. Hosokawa, M. Omata and M. Maeda, Anal. Chem. **79** (2007) 6000.

[7] C. L. Bliss, J. N. McMullin and C. J. Backhouse, Lab Chip **7** (2007) 1280.

[8] Y. Tanaka, K. Morishima, T. Shimizu, A. Kikuchi, M. Yamato, T. Okano and T. Kitamori, Lab Chip **6** (2006) 362.

[9] K. Hosokawa, M. Omata and M. Maeda, Anal. Chem. **79** (2007) 6000.

[10] C. L. Bliss, J. N. McMullin and C. J. Backhouse, Lab Chip **7** (2007) 1280.

[11] Y. Tanaka, K. Morishima, T. Shimizu, A. Kikuchi, M. Yamato, T. Okano and T. Kitamori, Lab Chip 6 (2006) 362.

[12] F. O. Lucas, A. Mitra, P. J. McNally, L. O'Reilly, S. Daniels, G. Natarajan and K. Durose, J. Mater. Sci. Mater. Electron. (online)

[13] H. Liang and R. G. Gordon, J. Mater. Sci. **42** (2007) 6388.

[14] M. Birnbaum, J. Appl. Phys. **363** (1965) 688.

[15] D. C. Emmony, R. P. Howson and L. J. Willis, Appl. Phys. Lett. **598** (1973) 23.

[16] J. F. Young, J. S. Preston, H. M. van Driel and J. E. Sipe, Phys. Rev. B **27** (1983) 1155.

[17] B. C. Stuart, M. D. Feit, A. M. Rubenchik, B. W. Shore and M. D. Perry, Phys. Rev. Lett. **74** (1995) 2248.

[18] B. C. Stuart, M. D. Feit, S. Herman, A. M. Rubenchik, B. W. Shore and M. D. Perry, Phys. Rev. B, **53** (1996) 1749.

[19] K. K. Thornber, AIP **52** (1981) 279.

[20] D. Arnold and E. Cartier, Phys. Rev. B **46** (1992) 15102.

[21] A. Kaiser, B. Rethfeld, M. Vicanek and G. Simon, Phys. Rev. B **61** (2000) 11437.

[22] E. Yablonovitch and N. Bloembergen, Phys. Rev. Lett. **29** (1972) 907.

[23] S. S. Mao, F. Quere, S. Guizard, X. Mao, R. E. Russo, G. Petite and P. Martin, Applied Physics A: Materials Science & Processing **79** (2004) 1695.

[24] N. Bloembergen, Journal of Quantum Electronics, IEEE **10** (1974) 375.

[25] S. K. Sundaram and E. Mazur, Nat. Mater. **1** (2002) 217.

[26] S. Bar-Ad, and D. S. Chemla, Mater. Sci. Eng. B. 48, (1997) 83.

[27] H. Kalt, and M. Rinker, Phys. Rev. B. **45** (1992) 1139.

[28] E. N. Glezer, Y. Siegel, L. Huang, and E. Mazur, Phys. Rev. B. **51** (1995) 9589.

[29] J. Solis, C. N Afonso, J. F. Trull, and M. C. Morilla, J. Appl. Phys. **75** (1994) 7788.

[30] S. Kanehira, K. Miura, K. Fujita, K. Hirao, J. Si, N. Shibata and Y. Ikuhara, Appl. Phys. Lett. **90** (2007) 3.

[31] Y. Shimotsuma, P. G. Kazansky, J. R. Qiu and K. Hirao, Phys. Rev. Lett. **91**

(2003) 4.

[32] M. Shen, J. E. Carey, C. H. Crouch, M. Kandyla, H. A. Stone and E. Mazur, Nano Letters **8** (2008) 2087.

Chapter 1

Formation of Micro-structuring with Femtosecond laser

1.1 History and Characteristics of Femtosecond Laser

In 1962, after the development of Q-switched lasers, the high-power sources of pulses 10-100 ns long became available. The generators of giant nanosecond optical pulses (with the power reaching 10-100MW at that time) extensively renovated many branches of laser physics.

The next great success, the penetration into the picosecond time scale, dates back to 1966-1968. At that time the longitudinal mode locking methods were suggested and realized in practice through constructing the first picosecond neodymium-glass lasers with power from 1 to 10GW. For the first time, the nonlinear-optics methods for compression and reshaping of picoseconds pulses were demonstrated. The picoseconds frequency-tunable parametric oscillators put into operation at the same time could span the visible and infrared regions. Thus, the utilization of fast electronic nonlinearity was shown to be efficient in picosecond and sub-picosecond optical systems.

Finally, in the early eighties several groups passed the 100 fs mark and the speedy development of femtosecond technology started. The first success came in 1981 when a new concept of a self-mode-locked dye laser was put forward, which was a system with pulses colliding in an absorbing medium. Later, the alternative mode-locking systems, other types of lasers, and various methods of nonlinear optics were successfully used for generation of femtosecond pulses. The time scale of a femtosecond becomes accessible

due to progress in the generation, amplification and measurement of ultrashort light pulses.

Based on the unique Characteristics of femtosecond pulses, Femtosecond technology opens up new fascinating possibilities. Large energy can be concentrated in a temporal interval as short as several 10^{-15}s which corresponds to only a few optical cycle in the visible range. The pulse peak power can be extremely large even at modulate pulse energies. For example, a 50 femtoseonds pulse with an energy of 1 mJ exhibits a peak power of 20 Gigawatt. An intensity of 20 Petawatt / cm^2 can be yielded focusing this pulse to a 100 μm^2 spot. The geometrical length of a femtosecond pulse amounts only to several micrometer. In particular, the availability of femtosecond pulse allows materials to be subjected to higher laser intensity than ever before, opening the door to the study of laser – material interactions in a new regime. Fundamental mechanisms responsible for the light – matter reaction in the time scale of a femtosecond will be discussed in the next section.

1.2 Fundamental of Light -Matter Nonlinear Interaction

Femtosecond laser results in the laser-induced optical breakdown, a process by which optical energy is transferred to the material, ionizing a large number of electrons that transfer energy to the lattice. As a result of the irradiation, the material can undergo a phase of structural modification, leaving behind a localized permanent change in the refractive index or even a void. It is difficult to produce an interaction effect between materials with big bandgap and light by a one-photon process when the wavelength of excitation light differs in the resonant absorption band of the materials. The absorption of light in the materials with big band-gap must be nonlinear because there are no allowed electronic transitions at the energy of the incident photon [1]. For such nonlinear absorption to occur, the electric-field strength in the laser pulse must be approximately equal to the electric field that binds the valence electrons in the atoms -of the order of 10^9 V m^{-1}, corresponding to a laser intensity of 5×10^{20} W m^{-2}. To achieve such electric-field strengths with a laser pulse, high intensities and tight focusing are required. For example, a 1-μJ, 100-fs laser pulse must be focused to a 200μm^2 area. The tight focusing and the nonlinear nature of the absorption make it possible to confine the absorption to the focal volume inside the bulk of the material without causing absorption at the surface, yielding micromachined volumes as small as 0.008 μm^3 [2].

During irradiation, the laser pulse transfers energy to the electrons through nonlinear ionization [1,3].

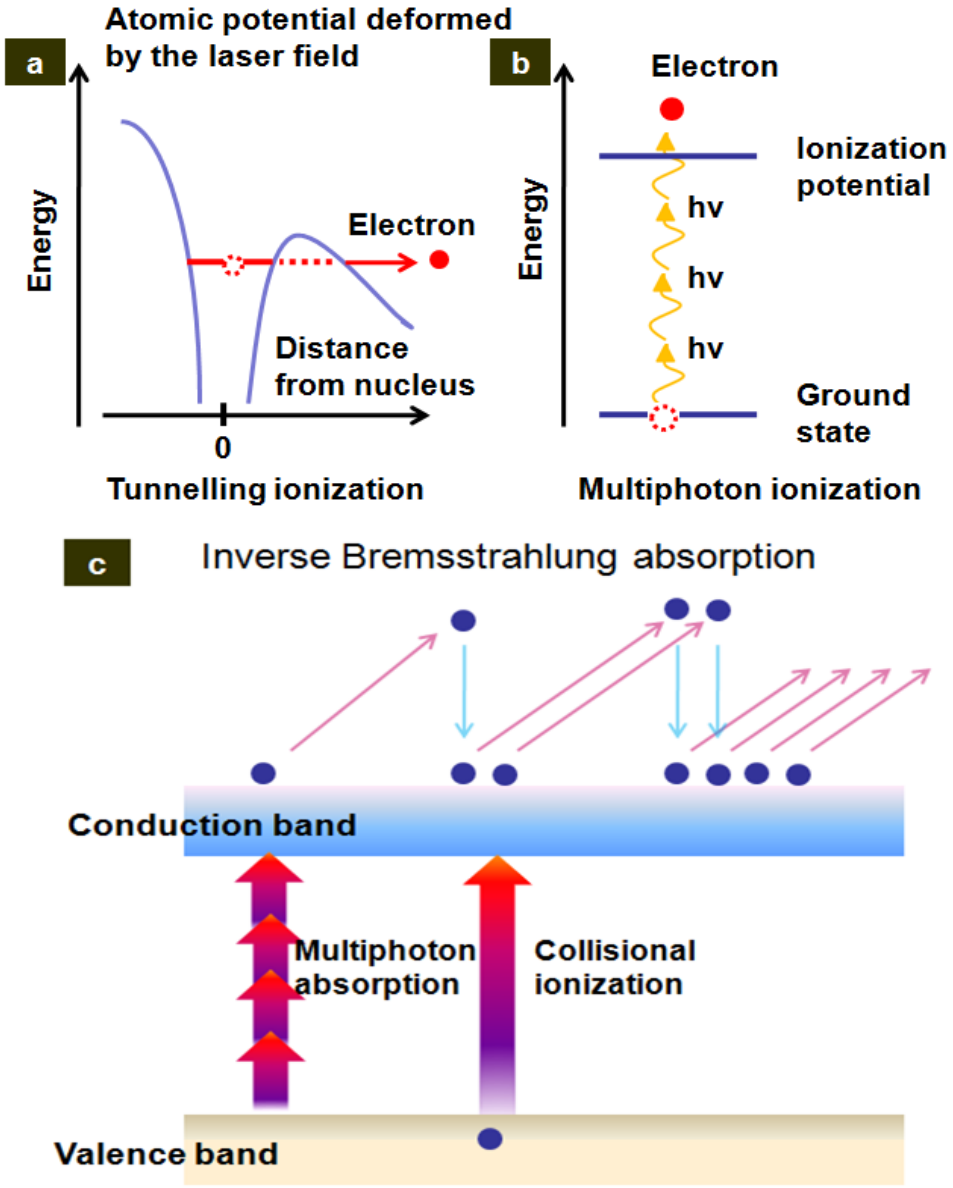

Figure 1. Schematic diagram of (a) Tunneling ionization and (b) Multiphoton ionization and (c) Avalanche ionization which shows an interplay of photonization, inverse Bremsstrahlung absorption, and collisional ionization.

Because a single photon of visible light does not have enough energy to excite an electron in a transparent material from the valence to the conduction band, multiple photons are required to excite the electron. Depending on the laser frequency and intensity, there are two different regimes of photoionization, the multiphoton ionization regime and the tunnelling ionization regime. Keldysh showed that both multiphoton and tunnelling regimes could be described within the same framework [4]. The conceptual picture and the approximations used in calculations for these two mechanisms are very different, however.

In tunneling ionization, the electric field of the laser suppresses the Coulomb well that binds a valence electron to its parent atom. If the electric field is very strong, the Coulomb well can be suppressed enough that the bound electron tunnels through the short barrier and becomes free, as shown schematically in the left-hand panel of figure 1(a). This type of nonlinear ionization dominates for strong laser fields and low laser frequency. At high laser frequencies, nonlinear ionization occurs due to the simultaneous absorption of several photons by an electron, as shown in the figure 1(b). To be promoted from the valence to the conduction band by this multiphoton absorption, the electron must absorb enough photons so that the number of photons absorbed times the photon energy is equal to or greater than the band-gap of the material.

For pulse durations greater than 10 femtosecond, the nonlinearly excited electrons are further excited through phonon-mediated linear absorption, until they acquire enough kinetic energy to excite other bound electrons -- a process called avalanche ionization. Avalanche ionization involves free-carrier absorption followed by impact ionization. An

electron already in the conduction band of the material linearly absorbs several laser photons sequentially, moving to higher energy states in the conduction band, so-called inverse Bremsstrahlung absorption as illustrated in Figure 1 (c). In order to conserve both energy and momentum, the electron must transfer momentum by absorbing or emitting a phonon or scattering off an impurity when it absorbs a laser photon. For electrons high in the conduction band, the deformation potential scattering time is approximately 1 femtosecond, so frequent collisions make free carrier absorption efficient [5]. After the sequential absorption of *n* photons, the electron's energy exceeds the conduction band minimum by more than the band-gap energy, where *n* is the smallest number which satisfies the relation $n\hbar\omega \geq Eg.$, and ω is the laser frequency, *Eg* is the band-gap of the material. The electron can then collisionally ionize another electron from the valence band, as illustrated "collisional ionization" in Figure 1 (c).

The result of the collisional ionization is two electrons near the conduction band minimum, each of which can absorb energy through free-carrier absorption and subsequently impact ionize additional valence band electrons. As long as the laser field is present, the electron density, *N*, in the conduction band grows according to

$$\frac{dN}{dt} = \eta N \qquad (1)$$

where η is the avalanche ionization rate.

Avalanche ionization requires some "seed" electrons in the conduction band of the material. These initial electrons are provided either by thermally excited carriers, by easily ionized impurity or defect states, or by carriers that are directly photo-excited by

multiphoton or tunnelling ionization. When the density of excited electrons reaches about 10^{29} m^{-3}, the electrons behave as the plasma with a natural frequency that is resonant with the laser – leading to reflection and absorption of the remaining pulse energy [6].

1.3 Damage mechanisms of Light - Matter Interactions

Figure 2 shows the timescales for a number of relevant physical processes involved in femtosecond laser micromachining. Part of the optical energy absorbed by the electrons is transferred to the lattice over a picosecond timescale. Within a couple of nanoseconds, a pressure or a shock wave separates from the dense, hot focal volume [7-9]. On the microsecond timescale, the thermal energy diffuses out of the focal volume. At a sufficiently high energy these processes cause melting or non-thermal ionic motion and leave behind permanent structural changes [10].

Laser-induced damage has been studied since the early days of the laser [5], but damage caused by femtosecond laser pulses is fundamentally different from damage caused by laser pulses with a duration greater than one picosecond. For pulse durations longer than a few tens of picoseconds, energy is transferred from the laser-excited electrons to the lattice on the time scale of the pulse duration. This energy is then carried out of the focal volume by thermal diffusion. Damage occurs when the temperature of the material in the irradiated region becomes high enough for the material to melt or fracture [11]. Energy is deposited into the material by the laser pulse and is transported out of the irradiated region by thermal diffusion, thus it is the relative rate of energy deposition and thermal diffusion that determines the damage threshold. Simple calculations show that, in this case, the threshold fluence for optical damage scales as the square root of the pulse duration.

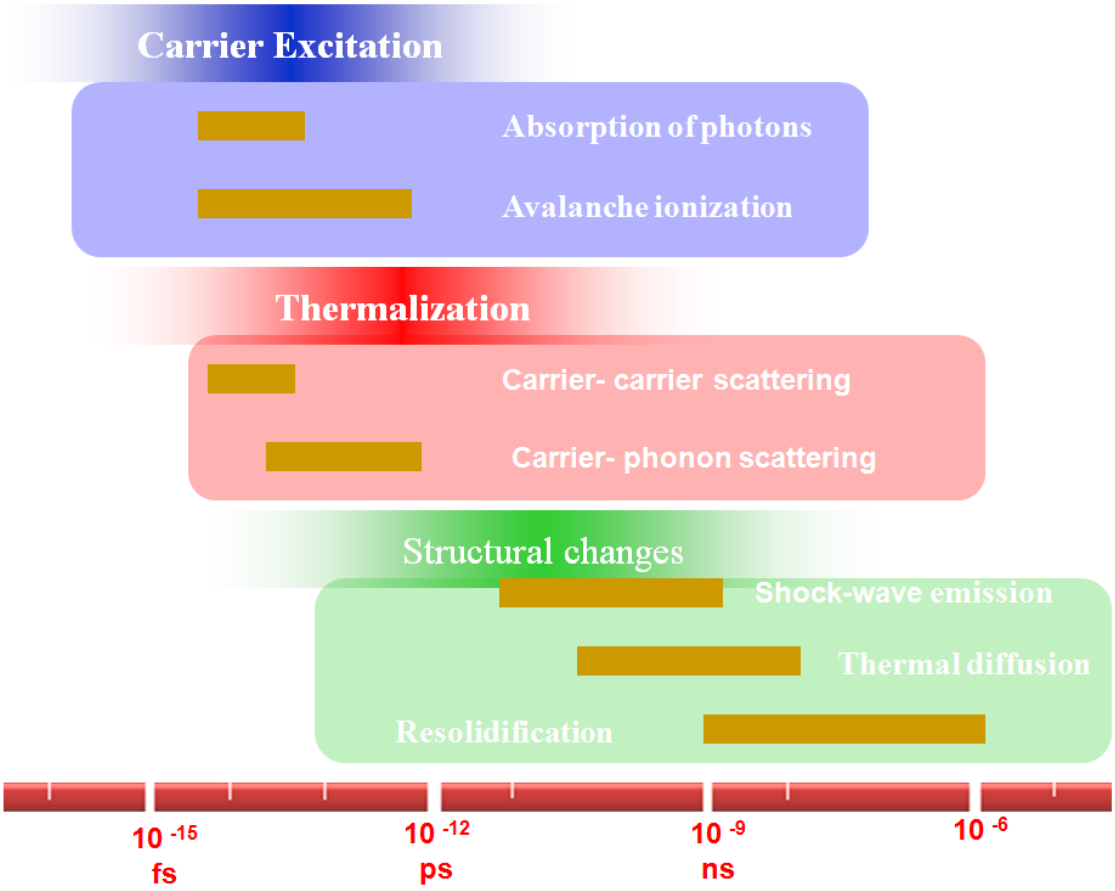

Figure 2. Timescale of the Physical phenomena associated with the interaction of a femtosecond laser pulse in materials.

For damage caused by pulses longer than a few tens of picoseconds, the source of the initial conduction-band electrons that seed the avalanche ionization is very important. Avalanche ionization is very efficient for such pulses because the long pulse duration allows more time for exponential growth of the electron density. Because avalanche ionization is so efficient, the laser intensity required to produce damage is not high enough to directly photoionizing electrons, so either thermally excited electrons or impurity and defect states provide the initial seed electrons for the avalanche. A high concentration of easily ionized impurity electrons lowers the threshold for optical damage compared to that of the pure material, making determination of the intrinsic breakdown threshold difficult [12].

For pulses shorter than a few picoseconds, the mechanism for optical damage is simpler than for longer laser pulses. Absorption occurs on a time scale that is short compared to the time scale for energy transfer to the lattice, decoupling the absorption and lattice heating processes [3]. Electrons in the conduction band are heated by the laser pulse much faster than they can cool by phonon emission. The electron density grows through avalanche ionization until the plasma frequency approaches the frequency of the incident laser radiation (the "critical" plasma density) [3]. This high density plasma strongly absorbs laser energy by free-carrier absorption. The reflectivity of the plasma at the critical density is only a few percent, so most of the laser energy is transmitted into the plasma where it can be absorbed. At higher plasma densities, however, a significant fraction of the laser pulse energy can be reflected. Only after the laser pulse is gone, energy transferred from the electrons to the lattice. This shock-like

deposition of energy, on a time scale much shorter than the thermal diffusion time, leads to ablation of material on the surface or permanent structural change in the bulk.

For sub-picosecond laser pulses, photoionization plays an important role in the generation of conduction band electrons. Photoionization by the leading edge of the laser pulse provides the seed electrons for avalanche ionization during the rest of the pulse [3]. This self-seeded avalanche makes short-pulse breakdown less dependent on defects in the material than long pulse breakdown and therefore the threshold for short-pulse damage is deterministic [12]. For very short laser pulses, photoionization can dominate avalanche ionization and produce a sufficient plasma density to cause damage by itself [3, 13].

Damage produced by pulses in the femtosecond range is far more regular from shot to shot and more confined than with longer pulses [2]. Because short pulses require less energy than longer pulses to reach the intensity necessary for producing optical breakdown, they deposit less energy in the material. Less energy deposition leads to more precise ablation or bulk material modification. This deterministic breakdown and damage near threshold and controllable material alteration make femtosecond lasers an ideal tool for micromachining [14].

1.4 Innovative Applications of Light-Matter Interaction with a Femtosecond Laser

The ultrafast laser has been used as a powerful tool to clarity elementary processes, such as excitation-energy relaxation and both electron and proton transfer on nanosecond and picoseconds time scales that occur in a micrometer-sized area. In the past decades, the ultrafast laser has been widely used in micro processing. A femtosecond laser, which is the typical ultrafast laser, has two apparent features compared with CW and long pulsed laser: (1) elimination of the thermal effect due to extremely short energy deposition time, and (2) participation of various nonlinear processes enabled by strong localization of laser photos in both time and spatial domains. Due to the ultrashort light-matter interaction time and the high peak power density, material processing with the femtosecond laser is generally characterized by the absence of heat diffusion and consequently molten layers [15]. The photo-induced reactions are expected to occur only near the focused part of the laser beam due to multiphoton processes. In the past several years, much research has been devoted to the field of three-dimensional microscopic modifications to transparent materials by using femtosecond laser. Promising applications have been demonstrated for the formation of 3D optical memory [16,17] and multicolor images [18], the direct writing of optical waveguides [19,20], waveguide couplers and splitters [21,22], waveguide optical amplifiers [23], and optical micro-gratings [24,25], Furthermore, in the recent applied researches, femtosecond lasers have been used as a fabrication method for a photonic crystals [26,27]. To micromachine a transparent material in three-dimensions, a

femtosecond laser beam is tightly focused into the bulk of the material. High laser intensity in the focal volume induces nonlinear absorption of laser energy by the material via multiphoton, tunneling, and a valanche ionization [28,29]. If sufficient laser energy is deposited, permanent structural changes are produced inside a material at the location of the laser focus. Depending on laser, focusing, and material parameters, different mechanisms may play a role in producing the structural changes and lead to different morphologies due to density and refractive index modification, to color centers generation, and to void formation [30].

Not only the femtosecond laser has been widely applied to micrometer-sized area, but also in the field of nanotechnology it can be widely used. The size and shape of nanoscale materials provide important control over many of the physics and chemical properties, including electric and thermal conductivity, luminescence, and catalytic activity [31]. Colloidal chemisits have obtained excellent controlled nanosized particles for several spherical metal and semiconductor compositions, which has led to the discovery of the quantum size effect in colloidal nancrystals [32]. However, various bottom-up approaches for making anisotropic-shaped colloidal nanoparticles have been found, with most of these solution methods being based on a thermal process. On the other hand, top-down approaches have been developed for producing metal and semiconductor nanowires, nanobelts, and nanoprisms [33-35]. In particular, the laser-induced ablation method has become an increasingly popular approach for making nanoparticles from the viewpoint of the concise procedure and application of a variety of materials [36-41]. The ripple structures have been observed on the surface of the

metal and semiconductor cause by the interferences between the scattering incident laser field and the surface Plasmon-polariton waves (SPWs) [41-45]. And Y. Shimotsuma etc. have reported the observation of the photoconversion from copper flakes to nanowires even nanospheres formation via ultrafast pulse laser irradiation in ethanol.

1.5 Conclusion

Femtosecond laser has been used to fabricate micro devices using a variety of materials including glasses, crystals and metal. It presents unique capabilities for three-dimensional, material in dependent, sub-wavelength processing. It enables the fabrication of three-dimensional photonic devices with far greater ease than lithography, and the field is maturing at an extraordinary pace. And a new method that the laser-induced ablated has become an increasingly popular approach for making nanoscale materials from the viewpoint of the concise procedure and application of a variety of materials. Because femtosecond laser micromachining also holds great promise beyond the field of photonics, it is a technology that creates new markets for the laser industry and enables innovative applications.

References

[1] B. S. Chris, B. Andre and M. Eric, Meas. Sci. Technol. **12** (2001) 1784.

[2] E. N. Glezer, C. B. Schaffer, N. Nishimura and E. Mazur, Opt. Lett. **22** (1997) 1817.

[3] B. C. Stuart, M. D. Feit, S. Herman, A. M. Rubenchik, B. W. Shore and M. D. Perry, Phys. Rev. B **53** (1996) 1749.

[4] L. V. Keldysh, Soviet Physics Jetp- Ussr **20** (1965)1307.

[5] N. Bloembergen, Journal of Quantum Electronics, IEEE **10** (1974) 375.

[6] B. C. Stuart, M. D. Feit, A. M. Rubenchik, B. W. Shore and M. D. Perry, Phys. Rev. Lett. **74** (1995) 2248.

[7] C. B. Schaffer, N. Nishimura, E. N. Glezer, A. M. T. Kim and E. Mazur, Opt. Express **10** (2002) 196.

[8] M. Sakakura and M. Terazima, Phys. Rev. B **71** (2005) 2.

[9] M. Sakakura, M. Terazima, Y. Shimotsuma, K. Miura and K. Hirao, Opt. Express **15** (2007) 5674.

[10] S. K. Sundaram and E. Mazur, Nat. Mater. **1** (2002) 217.

[11] B. C. Stuart, M. D. Feit, S. Herman, A. M. Rubenchik, B. W. Shore and M. D. Perry, J. Opt. Soc. Am. B **13** (1996) 459.

[12] D. Du, X. Liu, G. Korn, J. Squier and G. Mourou, Appl. Phys. Lett. **64** (1994) 3071.

[13] M. Lenzner, J. Kruger, S. Sartania, Z. Cheng, C. Spielmann, G. Mourou, W. Kautek, and F. Krausz, Phys. Rev. Lett. **80** (1998) 4076.

[14] X. Liu, D. Du and G. Mourou, IEEE Journal of Quantum Electronics, **33** (1997)

1706.

[15] B. N. Chickov, C. Momma, S. Nolte, F.V. Alvensleben and A. Tunnermann, Appl. Phys. A **63** (1996) 109.

[16] E.N. Glezer, M. Milosavljevic, L. Huang, R. J. Finlay, T. H. Her, J. P. Callan and E. Mazur, Opt. Lett. **21** (1996) 2023.

[17] J. Qiu, K. Miura and K. Hirao, Jpn. J. Appl. Phys. **37** (1998) 2263.

[18] J. Qiu, K. Miura, H. Inouye, Y. Kondo, T. Mutsuyu and K. Hirao, Appl. Phys. Lett. **73** (1998) 1963.

[19] K. Hirao and K. Miura, Jpn. J. Appl. Phys. **37** (1998) L49.

[20] M. Will, S. Nolte, B.N. Chichkov and A. Tunnermann, Appl. Opt. **41** (2002) 4360.

[21] D. N. Fittinghoff, C. B. Schaffer, E. Mazur and J. A. Squier, IEEE J. Sel. Top. Quantum Electron. **7** (2001) 559.

[22] K. Minoshima, A. M. Kowalevicz, I. Hartl, E. P. Ippen and J.G Fujimoto, Opt. Lett. **26** (2001) 1516.

[23] Y. Sikorski, A. A. Said, P. Bado, R. Maynard, C. Flotea and K.A. Winick, Electron. Lett. **36** (2000) 226.

[24] K. Miura, J. Qiu, T. Mitsuyu and K. Hirao, Nucl. Instr. and Meth. in Phys. Res. B **141** (1998) 726.

[25] Y. Kondo, K. Nouchi, T. Mitsuyu, M. Watanabe, P. G. Kazansky and K. Hirao, Opt. Lett. **24** (1999) 646.

[26] B. H. Cumpston, S. P. Ananthavel, S. Barlow, D. L. Dyer, J. E. Ehrlich, L. L. Erskine, A. A. Heikal, S. M. Kuebler, I. Y. S. Lee, D. Mccord-Naughton, J. Qin, H.

Rokel, M. L. Wu, S. R. Marder and J. W. Petty, Nature **398** (1999) 51.

[27] H. B. Sun, Y. Xu, S. Joudkazis, K. Sun, M. Watanabe, J. Nishii, S. Matsuo and H. Misawa, Opt. Lett. **26** (2001) 325.

[28] B. C. Stuart, M. D. Feit, S. Herman, A. M. Rubenchik, B. W. Shore and M. D. Perry, Phys. Rev. B **53** (1996) 1749.

[29] M. Lenzner, L. J. Kruger, S. Sartania, Z. Cheng, C. Spielmann, L. G. Mourou, W. Kautek and F. Krausz, Phys. Rev. Lett. **80** (1998) 4076.

[30] Y. Shimotsuma, J. Qiu, P. G. Kazansky and K. Hirao, Proc. SPIE **5662** (2004) 173.

[31] C. M. Lieber and Solid State Commun, **107** (1998) 607.

[32] A. P. Alivisatos, Science **271** (1996) 933.

[33] J. T. Hu, T. W. Odom and C. M. Lieber, Acc. Chem. Res. **32** (1999) 435.

[34] Z. W. Pan, Z. R. Dai and Z. L. Wang, Science **291** (2001) 1947.

[35] R. Jin, Y. W. Cao, C. A. Mirkin, K. L. Kelly, G. C. Schatz and J. G. Zheng, Science **294** (2001) 1901.

[36] J. P. Sylvestre, A. V. Kabashin, E. Sacher, M. Meunier and J. H. Luong, J. Am. Chem. Soc. **126** (2004) 7076.

[37] M. Kawasaki and K. Masuda, J. Phys. Chem. B **109** (2005) 9379.

[38] Y. Tamaki, T. Asahi and H. Masuhara, J. Phys. Chem. A **106** (2002) 2135.

[39] S. Link, C. Burda, M. B. Mohamed, B. Nikoobakht and M. A. EI-Sayed, J. Phys. Chem. A **103** (1999) 1165.

[40] B. R. Tull, J. E. Carey, M. A. Sheehy, C. Friend and E. Mazur, Appl. Phys. A: Mater. Sci. Process. **83** (2006) 341.

[41] T. Q. Jia, F. L. Zhao, M. Huang, H. X. Chen, J. R. Qiu, R. X. Li, Z. Z. Xu and H. Kuroda, Appl. Phys. Lett. **88** (2006) 111117.

[42] S. R. Brueck and D. J. Ehrlich, J. Phys. Rev. Lett. **48** (1982) 1678.

[43] A. Vorobyev, V. Makin, and C. Guo, J. Appl. Phys. **101** (2007) 034903.

[44] J. Wang and C. Guo, Appl. Phys. Lett. 87 (2005) 251914.

[45] A. Vorobyev and C. Guo, Appl. Phys. A: Mater. Sci. Process. 86 (2007) 321

Chapter 2

Selective Metallization of Ag_2O-doped Silicate Glass by Femtosecond Laser Direct Writing

2.1 Introduction

In recent years, femtosecond laser microfabrication has received significant attention for its capability of making various functional microcomponents into a single substrate, so providing a new way to fabricate highly integrated microdevices such as lab-on-a-chips [1] and micro-total-analysis-system (μ-TAS) [2-5] devices which allow chemical reactions and biomedical analysis to be performed within a small sample [6-8]. For example, μ-TAS is composed of some microfluidic components (such as micropumps, microvalves and micromixers) produced by a glass chip with a size of the order from 1 to 10000 of mm^2. Based on μ-TAS, infusion, flow switching, particle separation, mixing, pumping, reaction of reagents and the analysis of reactants could be successively conducted. However, the electrical control of such a mechanical component by electromagnetic force is more desirable for accurate operation in μ-TAS applications. Thus, the development of a technique enabling the selective metallization on a glass substrate assumes even greater importance. One preparation strategy for μ-TAS devices is to use vacuum evaporation [9] or chemical vapor deposition (CVD) [10] to deposit metal thin films on a glass chip, but these methods are complicated and onerous in view of a needed resist process and vacuum for photolithography in micropatterning. Laser direct writing is expected to be an alternative method of forming

patterns on metal thin films without photolithography. In this work, we report a simple and convenient technique for selective metallization of Ag_2O-doped silicate glass by the Femtosecond Laser direct writing with electroless copper plating.

2.2 Experimental

The experimental setup was in the following for making the silicate glasses of $70SiO_2 \cdot 10CaO \cdot 20Na_2O$ doped with Ag_2O (0.05mol%). Reagent grade SiO_2, $CaCO_3$, Na_2CO_3, and Ag_2O were used as starting materials. Approximately 30 g batches were mixed and melted in platinum crucibles in an electronic furnace at 1600^oC for 1 hour under the ambient atmosphere. The melts were then quenched to room temperature to obtain transparent and colorless glasses. Ag_2O-doped glass was irradiated by using amplified Femtosecond Laser pulses (250 kHz, 70 fs, 800 nm) of a mode-locked Ti-sapphire laser oscillator (Coherent; Mira and RegA). The Femtosecond Laser pulses were attenuated by a neutral density filter and focused on the surface of soda lime glass plate (Schott B 270 Superwite) through a 20× objective lens (NA=0.40; Nikon LU Plan ELWD 20). The glass sample was put on a computer-controlled XYZ stage, and the laser writing process was directly performed in air. The optical setup of femtosecond laser used in our experiment is shown in Figure 1. Then, electroless copper (Cu) plating is carried out at room temperature for 20 min using a mixture of Cu-ion solution containing $CuSO_4$ 30 g/L, sodium potassium tartrate 100 g/L, NaOH 50 g/L, and formaldehyde 30 mL/L aqueous solution of formaldehyde (37.2 wt.%). It is indispensable that the Ag_2O-doped silicate glass should be rinsed in deionized water after each step.

Using optical microscopy, we investigate the morphology of the Ag_2O-doped silicate glass sample. After the Femtosecond Laser irradiation, the surface of the sample was analyzed by a X-ray photoelectron spectroscopy (XPS, ULVAC-PHI, Inc.).The

exciting X-ray used for XPS was MgKα, 1254ev, and 400W. And the surface of electroless plating sample was analyzed by an electron probe micro-analyzer (EPMA, JEOL, JXA-8900-RL). All of the experiments were carried out at room temperature.

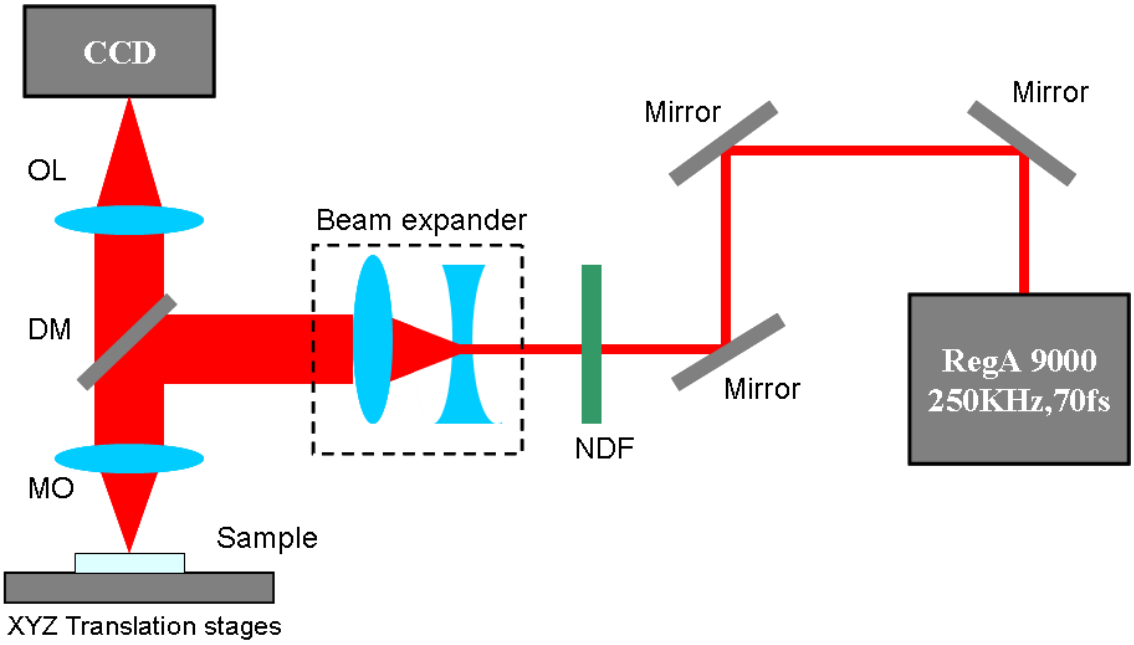

Figure 1. Schematic of the femtosecond laser setup. Beam expander is composed of a convex lens and a concave lens. DNF: neutral density filter; MO: microscope objective; DM: dichroic mirror. OL: optical lens.

2.3 Results and discussion

The glass substrate was ablated at a laser power of 50~400mW and a laser scanning speed of 50μm/s. The resulted line widths of the groove are estimated to be about 2~8μm. To verify the state of irradiation region, extinction spectrum and XPS was employed.

We measure absorption spectra in the wavelength range from 200 to 800nm using a spectrophotometer before and after the focused irradiation of femtosecond Laser. Since the focal volume was too small to detect the absorption change using a spectrophotometer, we increased the irradiation area by scanning. Then we used scanning irradiation to produce irradiated lines in the surface of Ag_2O doped silicate glass by using a 20 × objective lens (NA 0.40) and translating the samples perpendicular to the incident laser beam at a rate of 50μm/s with a line period of 100μm. The pulse energy was 200mW.

Figure 2. shows the extinction spectra of the glass sample before (a) and after (b) the laser irradiation. No obvious absorption was observed for the non-irradiation glass sample in the wavelength region from 600nm to 800nm, while there was a significant absorbance from 200nm to 600nm wavelength in the irradiated region. The inset of Figure 2, shows the difference in extinction spectrum of the Ag_2O-doped glass (0.05mol%) before and after the Femtosecond Laser irradiation.

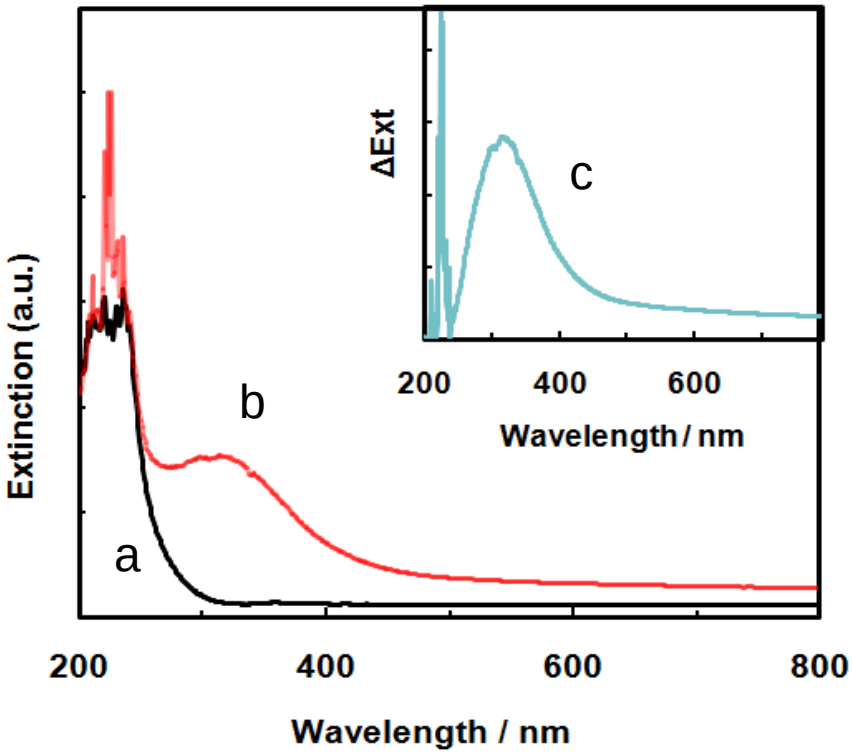

Figure 2. Extinction spectra of Ag_2O-doped glass (0.05mol%) (a) before and (b) after Femtosecond Laser irradiation. (c) Difference extinction spectrum of Ag_2O-doped glass (0.05mol%) before and after the Femtosecond Laser irradiation (inset of Figure)

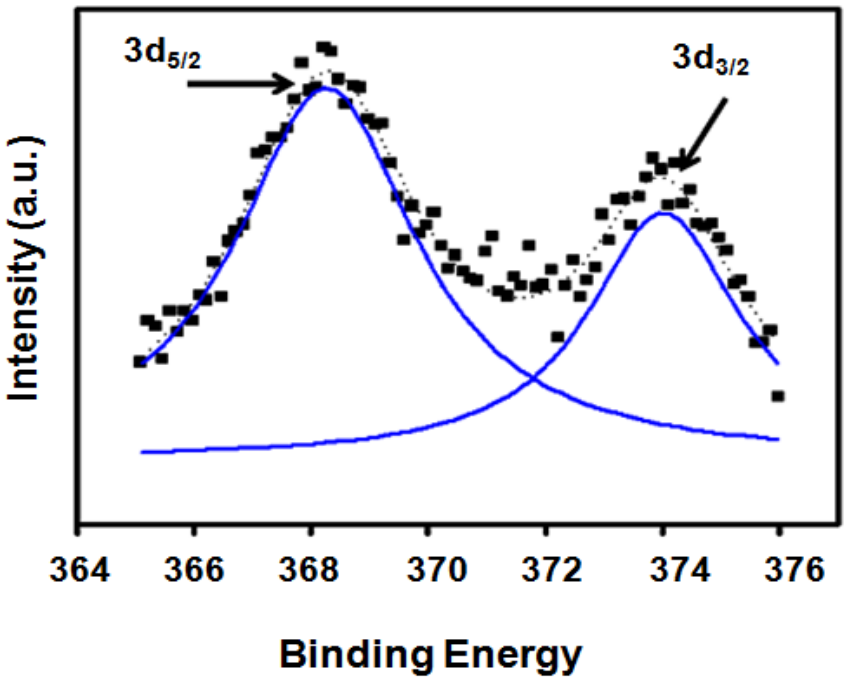

Figure 3. The XPS spectra of Ag 3d signals of the irradiated area in Ag_2O-doped glass. Blue curves are deconvolution results after fitting.

As demonstrated in Figure 2(c), the extinction peaks of 230nm and 330nm can be assigned to the atomic silver and hole trap centers at non-bridging oxygen near Ag^+ ions, respectively [12]. Meanwhile, from the XPS images (Figure 3) of the ablated Ag_2O-doped glass, we can assign Ag $3d_{5/2}$ and $3d_{3/2}$ to the binding energies of 368.2eV and 374.2eV, which exactly correspond to signals from atomic silver. All arguments are in good agreement with the preview data [11-13] and other published papers [14-18].

Therefore, according to the above results of extinction spectrum and XPS, it can be concluded that the non-bridging oxygen should act as hole-trap centers while the Ag^+ ions as electron-trap ones. In that case, after irradiation by Femtosecond Laser beam, an electron was driven out from the 2p orbital of a non-bridge oxygen in the SiO_4 polyhedron via the multiphoton absorption, while Ag^+ captured the electron to form an Ag atom. Consequently, the formation of silver atoms or even silver nanoparticles became the seeds for the subsequent electroless plating process.

Figure 4 shows FE-SEM images (a) and EPMA images(b, c and d) of as-ablated the Ag_2O-doped glass substrate after laser irradiation (power of 100mW and scanning speed of 50μm/s). The analysis of elements distribution in as-ablated area reveals that a large number of copper distributed in the middle of the area (Figure 4(b)), while silicon and oxygen mainly distributed on both sides of the area (Figure 4(c), (d)).

In other words, straight lines of Cu thin film are selectively deposited along the glass substrate on the irradiated lines.

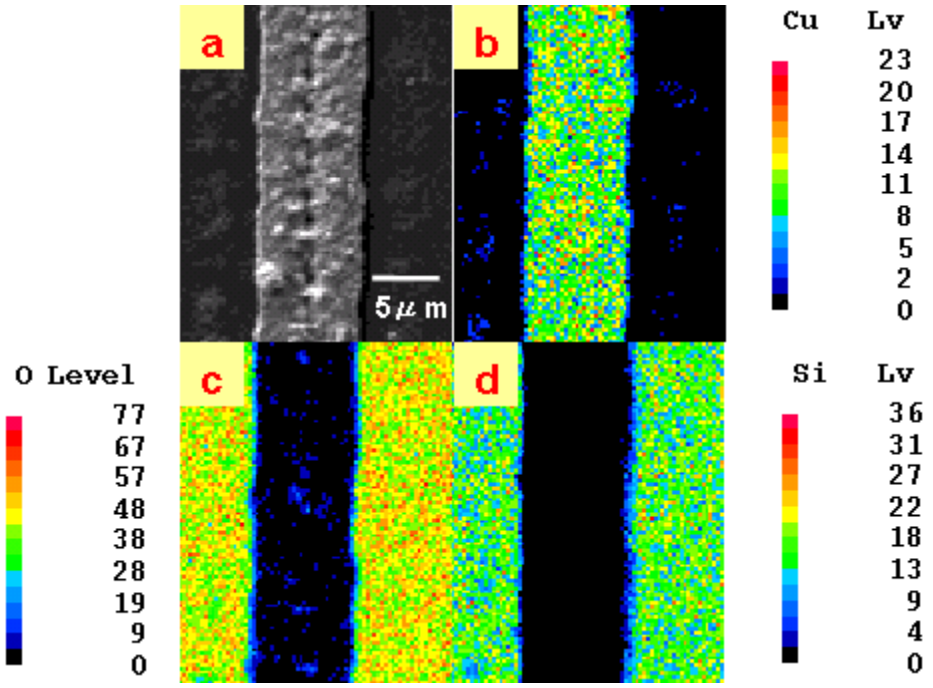

Figure 4. FE-SEM images (a) and EPMA images of (b) Cu, (c) O and (d) Si elements distribution after the irradiation. The laser power is 100 mW, and the laser scanning speed is set at 50μm/s.

Furthermore, we studied the dependences of the original ablated line-width and the followed plated Cu one on the laser power. As shown in Figure 4, the line widths of the irradiated region and the plated Cu increase from 2.5 to 7.5μm and from 7.4 to 25.4μm, respectively, as the laser power increases. The broader line width of the Cu film than the line ablated before is likely to be the result of isotropic growth of the Cu film.

Figure 6 shows the optical micrographs (a, b) and EPMA images (c, d, e and f) of several cross sections of the copper microstructures, after the electroless plating process, which was deposited in the Femtosecond Laser ablated grooves fabricated at a laser power of 100mW (a, c and e) and 200mW (b, d and f) with the same laser scanning speed of 50μm/s. The distributions of Cu and Si elements are shown in Figure 6(c), and 6(d), and Figure 6(e) and 6 (f), respectively. A large number of copper distributed in the middle of the area (Figure 6(c), (d)), while Silicon mainly distributed on both sides of the area (Figure 6(e), (f)). The cross-sectional shapes of copper microstructures indicated that the Cu films are deposited only in the ablated grooves area but not on the non-irradiated surfaces at all, which indicates that the silver atoms are generated only on the groove surface under laser irradiation.

Besides, the depth of laser ablated groove increased from 4.8 to 29μm, shown in Figure 7, with increasing the laser power. It is self-evident that the increase of groove depth will be beneficial for the fabrication of microelectrodes deeply embedded in transparent materials such as glasses or crystals. From the above discussion, we deduced a possible of selective metallization (Figure 8).

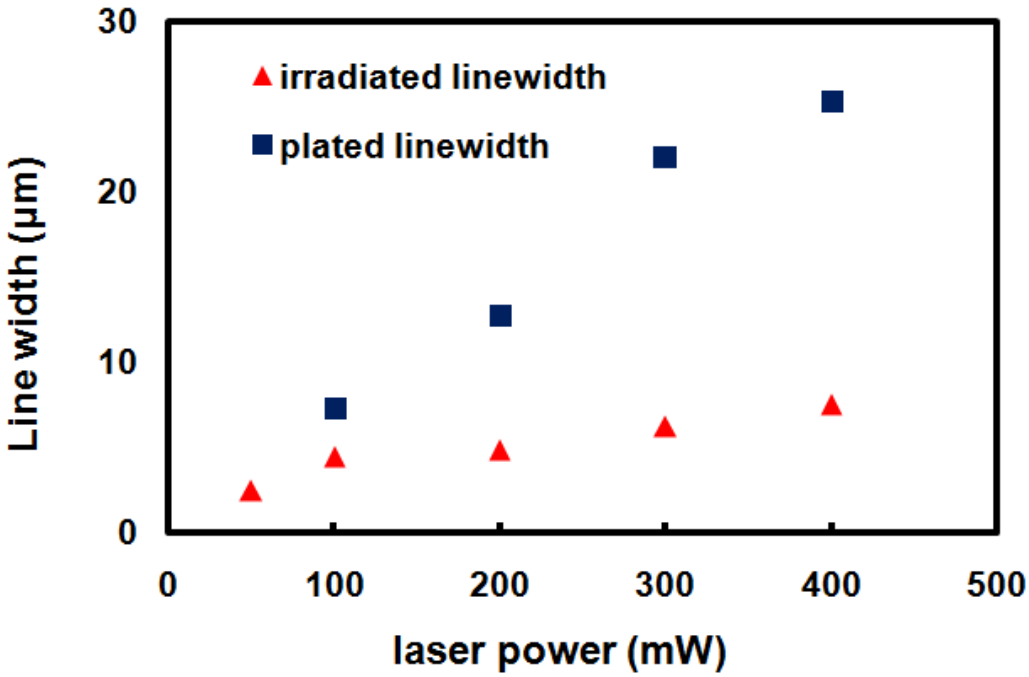

Figure 5. Dependences of irradiated and plated line widths on the laser powers.

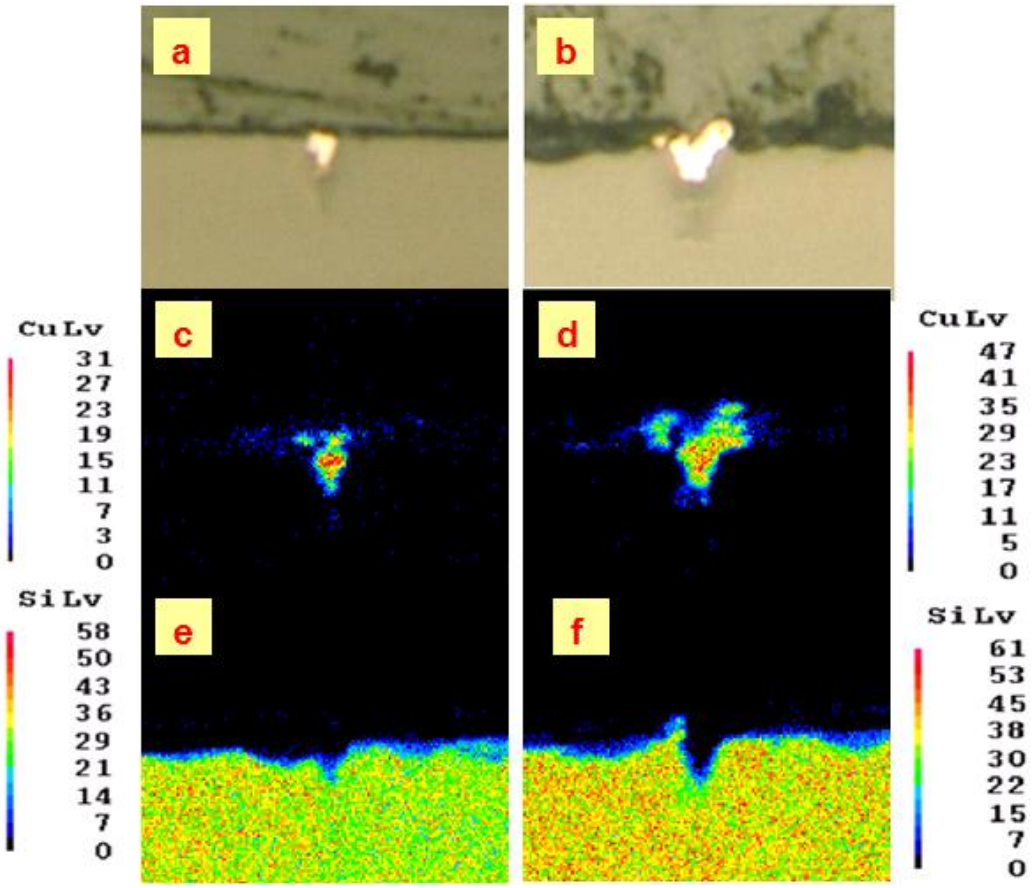

Figure 6. Optical micrographs (a, b) and EPMA images of Cu and Si distribution (c, d, e and f) on the cross sections of copper microstructures deposited inside the ablated grooves. The laser powers are100mW (a, c and e) and 200mW (b, d and f), and the laser scanning speed is set at 50μm/s.

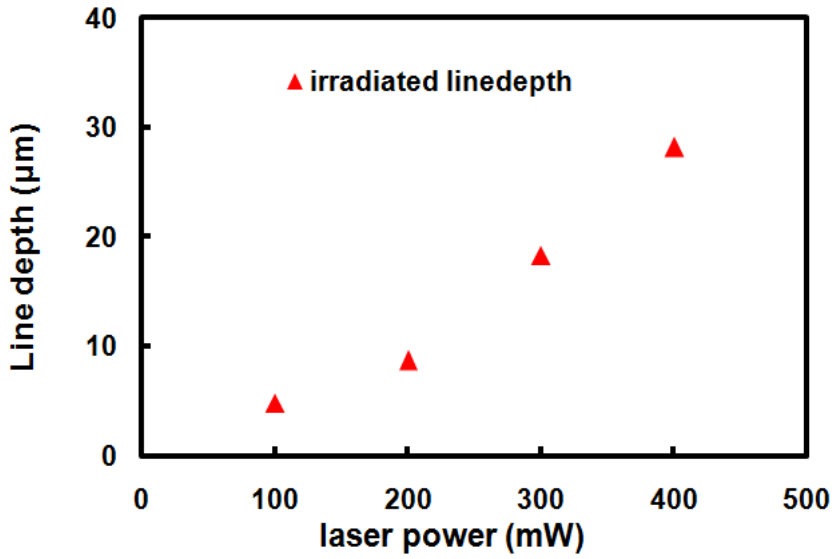

Figure 7. Dependences of irradiated line depths on the laser powers

When the Femtosecond Laser beam is focused on the surface of the Ag_2O-doped glass, an electron was driven out from the 2p orbital of a non-bridging oxygen in the SiO_4 polyhedron via the multiphoton absorption only at the focused region. The Ag ions near the non-bridging oxygen captured the free electrons and were reduced to Ag atoms on the surface of Ag_2O-doped glass, as demonstrated in Figure 8(a). Consequently, the formation of silver atoms or even silver nanoparticles became the seeds for the subsequent electroless plating process. In the electroless plating solution, only near the laser-irradiated regions, Cu atoms deposit and finally aggregate into Cu thin film(Figure 8(b)).

As an application of this selective metallization technique, the fabrication of a microheater was demonstrated. For this purpose, the focused femtosecond laser beam was first scanned on the Ag-doped glass surface. Then, electroless Cu plating was performed on the ablated glass sample. Figure 9 shows a schematic diagram of the microheater fabricated on a Ag-doped glass surface (a), and the microscope images of the microheater after irradiated (b) and after plated copper for measuring the temperature of the microheater (c). From Figure 9c, it can be seen that the Cu thin film was deposited in a triangular wave pattern on the glass surface. After the fabrication of the microheater, a power supply was connected to both ends of the microheater using a silver adhesive agent. To measure the temperature of the miroheater, a laser thermometer was focused on the glass surface on which the microheater was fabricated.

Figure 10 shows the temperature dependence of the microheater on the voltage. The temperature on the increases almost linearly up to 80 ^{o}C as the voltage increases, which

meas that the temperature can be easily controlled. The maximum temperature of 80 ^{o}C is not sufficiently high for μ-TAS applications, but the maximum temperature can be increased by increasing the length of the Cu thin film.

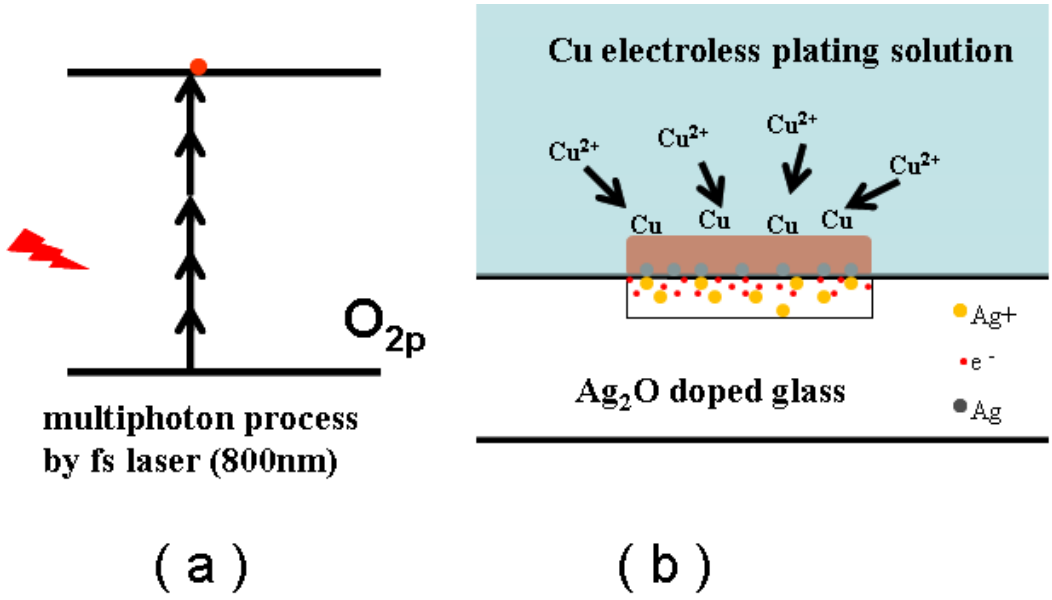

Figure 8. (a) Generation mechanism of free electrons in glass by the Femtosecond Laser for selective metallization. (b) Possible mechanism of the selective metallization of glass by electroless copper plating.

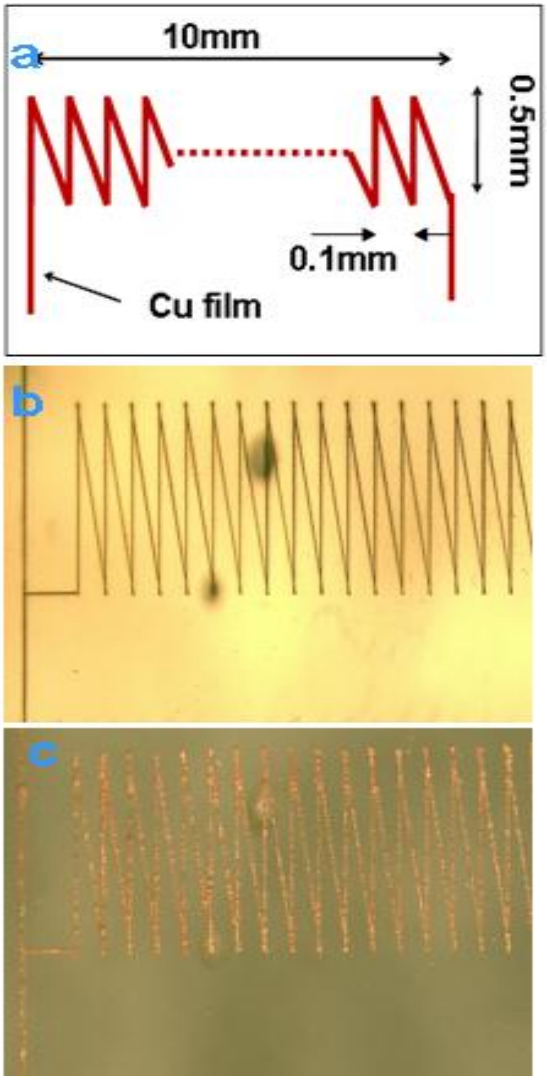

Figure 9. (a) Schematic diagram of a microheater, (b) microscope image of the microheater after irradiated and (c) microscope image of the microheater after plated copper for measuring the temperature of the microheater.

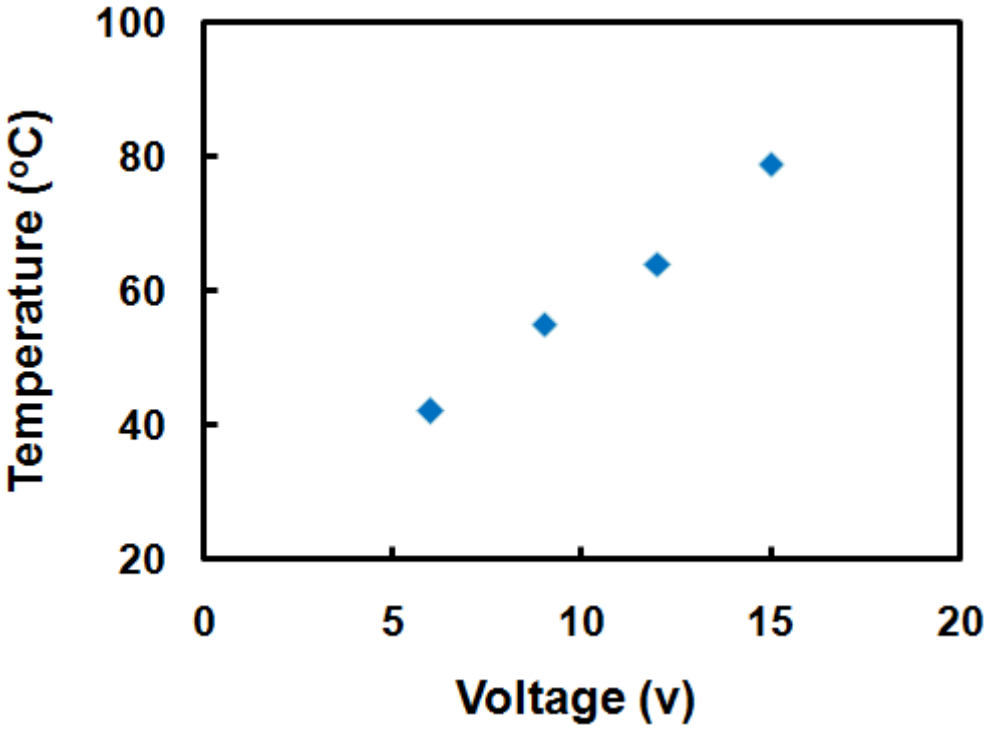

Figure 10. Dependence of temperature of the microheater on the voltage.

2.4 Conclusion

Due to the multiphoton reduction process, the reduction of an Ag ion to an atom by Femtosecond Laser irradiation is essential in forming Ag nanoparticles, and the Ag atom acts as a crystal nucleus for copper growth. The copper thin film can be deposited only on the irradiation regions, when electroless Cu plating process is performed. It was found that the line widths of the ablated region and the plated Cu increase from 2.5 to 7.5μm and from 7.4 to 25.4μm, the groove depths of the ablated region increase from 4.8 to 29μm, respectively, as the laser power increases.

References

[1] K. Sugioka, Y. Cheng and K. Midorikawa, Appl. Phys. A **81** (2005) 1.

[2] M. Masuda, K. Sugioka, Y. Cheng, N. Aoki, M. Kawachi, K. Shihoyama, K. Toyoda, H. Helvajian, and K. Midorikawa, Appl. Phys. A: Mater. Sci. Process. **76** (2003) 857.

[3] Y. Cheng, K. Sugioka, K. Midorikawa, M. Masuda, K. Toyoda, M. Kawachi, and K. Shihoyama, Opt. Lett. **28** (2003) 1144 .

[4] M. Masuda, K. Sugioka, Y. Cheng, T. Hongo, K. Shihoyama, K. Toyoda, H. Takai, I. Miyamoto, and K. Midorikawa, Appl. Phys. A: Mater. Sci. Process. **78** (2004) 1029

[5] Y. Cheng, K. Sugioka, and K. Midorikawa, Opt. Lett. **29 (**2004) 2007.

[6] K. Hosokawa, M. Omata and M. Maeda, Anal. Chem. **79** (2007) 6000.

[7] C. L. Bliss, J. N. McMullin and C. J. Backhouse, Lab Chip **7** (2007) 1280.

[8] Y. Tanaka, K. Morishima, T. Shimizu, A. Kikuchi, M. Yamato, T. Okano and T. Kitamori, Lab Chip 6 (2006) 362.

[9] F. O. Lucas, A. Mitra, P. J. McNally, L. O'Reilly, S. Daniels, G. Natarajan, K. Durose, Y. Y. Proskuryakov, D. C. Cameron: J. Mater. Sci. Mater. Electron. (online)

[10] H. Liang and R. G. Gordon, J. Mater. Sci. **42** (2007) 6388.

[11] J. Qiu, X. Jiang, C. Zhu, M. Shirai, J. Si, N. Jiang and K. Hirao, Angew. Chem. Int. Ed. **43** (2004) 2230.

[12] M. Tashiro and N. Soga, Kogyo Kagaku Zasshi **65** (1962) 342.

[13] B. Hua, J. Qiu, Y. Shimotsuma, K. Fujita and K. Hirao, J. Mater. Res. **20** (2005) 644.

[14] T. Hongo, K. Sugioka, H. Niino, Y. Cheng and M. Masuda, J. Appl. Phys. **97** (2005) 063517.

[15] T. Baldacchini, A. C. Pons, J. Pons, C. N. LaFratta, J. T. Fourkas, Y. Sun and M. J. Naughton, Opt. Express **13** (2005) 1275-1280.

[16] T. Tanaka, A. Ishikawa and S. Kawata, Appl. Phys. Lett. **88** (2006) 081107.

[17] S. Maruo and T. Saeki, Opt. Express **16** (2008) 1174.

[18] Y. Kondo, J. Qiu, T. Mitsuyu, K. Hirao and T. Yoko, Jpn. J. Appl. Phys. **38** (1999) L1146.

Chapter 3

Nano-periodic structure formation on titanium thin film with a Femtosecond laser

3.1 Introduction

High power ultrashort pulse lasers have opened new frontiers in technology of light−matter interactions, physics and chemistry fields. Its applications have expanded from coherent x-ray generation [1,2] and nonlinear Thomson scattering [3] to direct writing of 3D photonic structures [4−6]. One reason is femtosecond pulses, for direct writing and data storage, can rapidly and precisely deposit energy in solids [7−8] in contrast with longer ones.

Laser−induced periodic surface structures on solids have been the subject of extensive theoretical and experimental study. Especially the nanostructure formation after ultrashort laser pulses treatment attracts a lot of interest. So far, there are many reports about laser−induced periodic surface structures on metals [9] dielectrics and semiconductors [9−11]. For example, Vorobyev et al., has applied the femtosecond laser technique for generating laser−induced periodic surface structures on various metals [12−14], and the forming of these nanostructures is generally believed to be the result of local periodic enhancement triggered by excitation of surface Plasmon polarizations in surface layer [15−17]. To the best of our knowledge, until now, all the reported nanostructures only mentioned the nanostructures perpendicular to the laser polarization direction. Here, for the first time, we report the controlled preparation of the

nanostructures vertical or horizontal to the laser polarization direction by ablating once, and the combined nanostructures through ablating twice.

3.2 Experimental

Firstly, using an radio frequency sputtering (ULVAC, KIKO, Inc, RFS-200), we deposited a Ti thin film (200 nm thick) on one silicon wafer (1 cm thick) within pure N_2 gas under bias voltage of 100W. Then, for the ablation experiment, the laser radiation in Gaussian mode produced by regenerative amplified mode-locked Ti:sapphire laser (70 fs pulse duration, 250 kHz repetition rate) operating at a wavelength of 800 nm was focused via 20×(numerical aperture = 0:45) microscope objective into the silica glass samples placed on the XYZ piezotranslation stage, as illustrated in figure 1. The beam was focused on the interface of Ti /Si. The laser writing parameters were controlled by an electronic shutter, a variable neutral density filter, and a half-wave plate placed in an optical path of the laser beam. We produce nanostructures over a line by scanning the sample across the laser beam, and the femtosecond pulse energy was set in a range of 0.008~0.064 μJ, and the number of irradiated pulses used was in a range of 30~102, corresponding to the scanning speeds of 10000~3000μm/s. After laser irradiation, the surface of the irradiated sample was observed by scanning electron microscope (JEOL, model JSM-6700F). All experimental were performed in air.

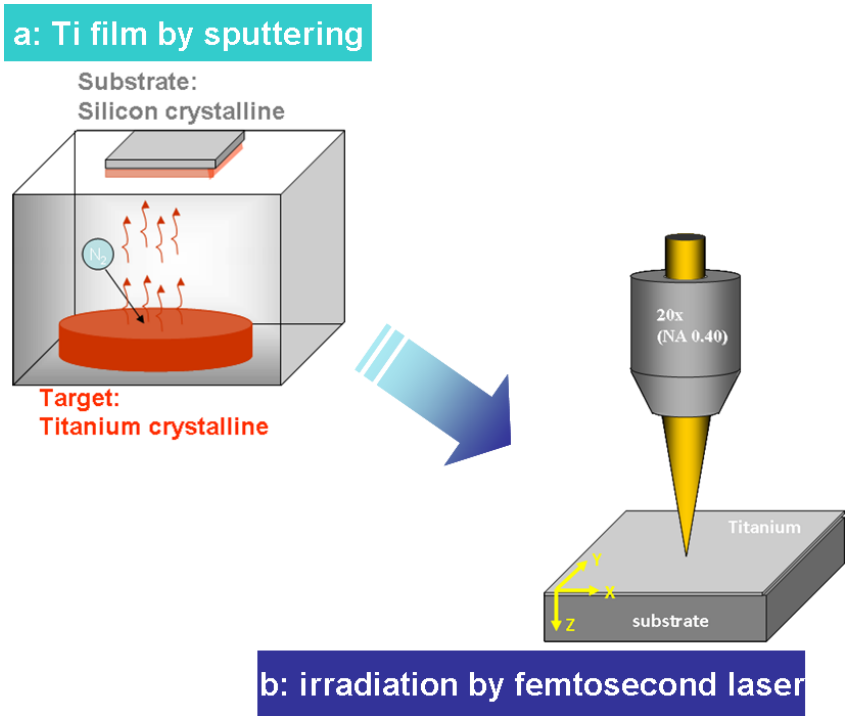

Figure 1. Schematic illustration of the fabrication process: (a) Ti film by sputtering and (b) irradiation by femtosecond laser.

3.3 Results and discussion

Figure 2 shows the SEM images of the Ti surface ablated by the femtosecond pulses (pulse energy 0.008 μJ and scanning speeds of 10000μm/s of linearly polarized output at 800 nm) with p− and s−polarizations. After ablation, the linearly polarized pulses produce fine slender ripple-like framework on the Ti film. This structure, with an average spacing of about 105 nm between the ripples, is highly oriented to the direction parallel to the laser polarization, differing the normal situation perpendicular to the laser polarization.

The difference may be interpreted as follows: once a high free electron density is produced by multi−photon ionization, the material has the properties of plasma and will absorb the laser energy via one−photon absorption mechanism of inverse bremsstrahlung (joule) heating, and the light absorption in the electron plasma will excite bulk electron plasma density waves. These are longitudinal waves with the electric field component parallel to the direction of propagation. Such an electron plasma wave could couple with the incident light wave only if it propagates in the plane of light polarization. Initial coupling is produced by inhomogeneities resulted from electrons′ moving in the plane of light polarization, which leads to the initial period distribution of the electron plasma concentration orientation parallel to the light polarization [18]. According to other early studies, if the electric field intensity does not exceed certain threshold, the structure of initial period distribution can be maintained without the risk of rupture [19].

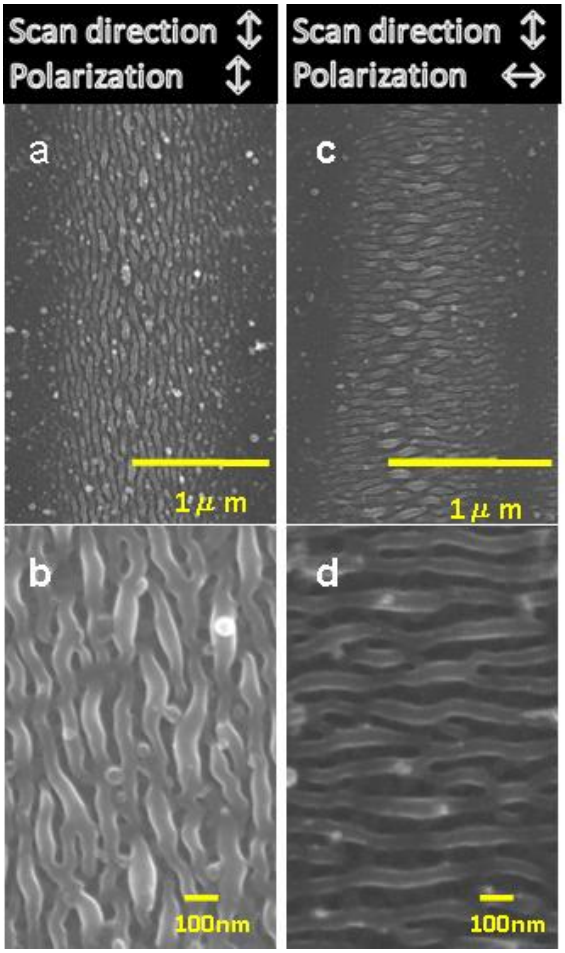

Figure 2. SEM images of the Ti surfaces ablated by the 800nm femtosecond laser pulses with P-polarization (a, b) and S-polarization (c, d). The magnification of the upper (a, c) and lower (b, d) images are 10000× and 50000×, repectively.

However, when the electric field intensity exceeds certain threshold, the further coupling is adequately increased by a periodic structure created via a pattern of interference between the incident light field and the electric field of the bulk electron plasma wave, resulting in the periodic modulation of the electron plasma concentration and the periodic structures oriented perpendicular to the light polarization [18]. Therefore, we have reason to consider this the ripple-like nanostructure oriented parallel to the light polarization was generated by the initial period distribution of the electron plasma concentration.

Figure 3(a) demonstrates a cross produced by two mutually perpendicular beams with scanning speeds of 10000μm/s and laser power of 0.016μJ. A closer observation shows that there are distinct morphologies in different ablation areas: the arms and the intersection. The same regular ripple-like nanostructures (as shown in Figure 3(b) and Figure 3(c)) with a periodicity of 91 nm exist in two arms areas, and the orientation of these ripple-like nanostructures are invariably parallel to the laser polarization. This result further confirms that the ripple orientation is strictly determined by the polarization of the incident laser. Figure 3(d) shows a net-like nanostructure fabricated in the two-beam overlapping area. The net-like structure can be referred to as the consequence of intercrossing of two orthogonal ripple-like nanostructures.

This means that the morphological characteristics of the corresponding ripple-like nanostructure induced by the beam with a certain polarization can be maintained in the ablation using the two-beam alternate ablation process.

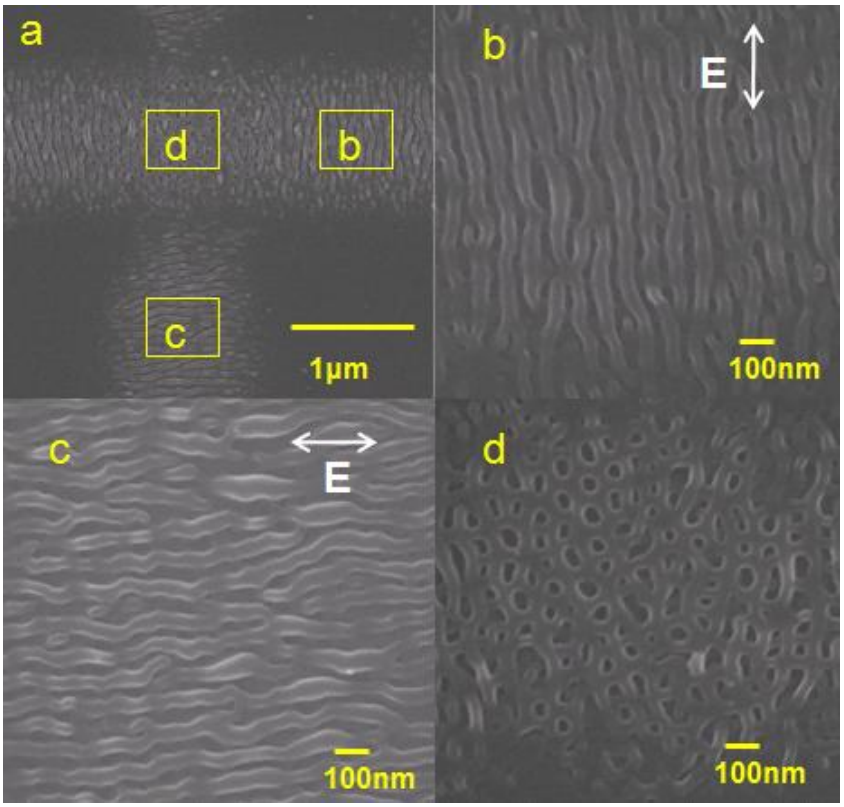

Figure 3. SEM images of a Ti surface ablated by the two-beam alternate ablation with scanning speeds of 10000μm/s and laser power of 0.016 μJ: (a) overview. (b) ripple-like nanostructure in the area ablated by one beam with vertical polarization. (c) ripple-like nanostructure in the area ablated by the beam with horizontal polarization. (d) net-like nanostructure formed in the two-beam overlapping area. Double arrows: the polarizations of the incident laser.

We found the period of ripple-like nanostructure is reversely related to the laser pulse number, as shown in Figure 4. Under same pulse energy of 8×10^{-3}μJ, the periods of 108, 96, and 85 nm are observed for the number of laser pulses of 31, 61, and 102 corresponding to the scanning speeds of 10000, 5000, 3000μm/s respectively. While fixing laser pulses number, the dependence of the observed periodic nanostructures on pulse energy reveals, shown in Figure 5, that the periods drop with the decrease of pulse energy. Periods of 108, and 91nm were measured at pulse energies of 8×10^{-3}μJ and 16×10^{-3}μJ, respectively, with a fixed number of laser pulses of 31.

For the simple Drude model [20] in which the damping is ignored, ε1 in the laser field is given by

$$\boldsymbol{\varepsilon_1 = \varepsilon_0 \times \left[\varepsilon_{Ti} - \left(\frac{{\omega_p}^2}{\omega^2}\right)\right]} \qquad (1)$$

Where ε_0 and ε_1 are the dielectric constants of vacuum and the Ti thin layer including the effect of free electrons. And the ε_{Ti} is the static relative dielectric constant of Ti with $\varepsilon_{Ti} = i\times25.7 - 5.78$ [21] and the ω is the angular frequency of the laser, respectively.

The plasma frequency ω_p is given by

$$\boldsymbol{\omega_p = \left[\frac{e^2 N_e}{\varepsilon_0 m}\right]^{\frac{1}{2}}} \qquad (2)$$

where e is electron charge and m is mass.

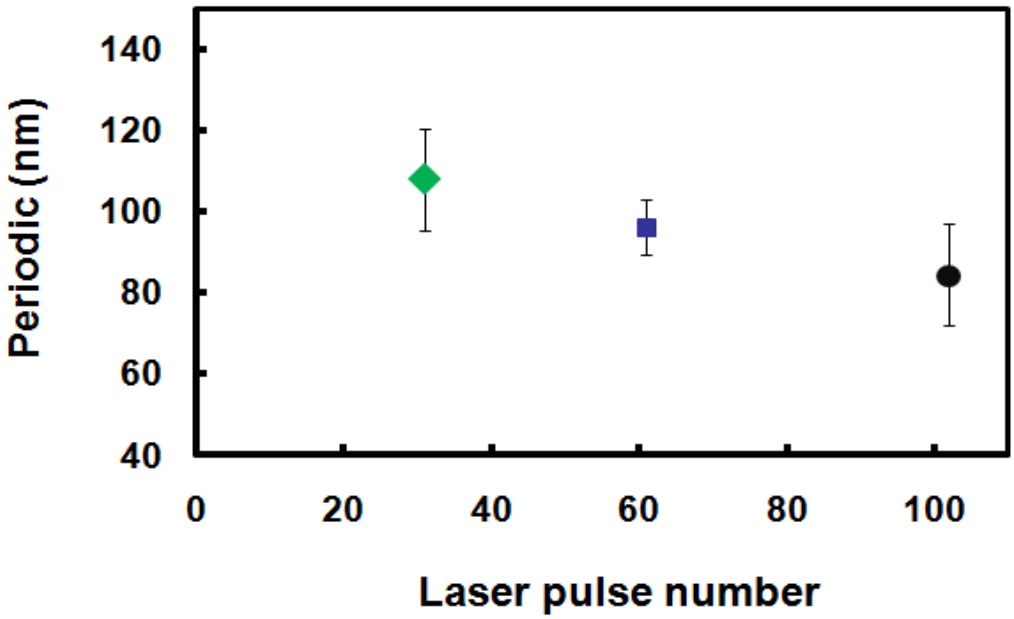

Figure 4. The dependence of the observed periodic nanostructures on the laser pulse number under a fixed pulse energy.

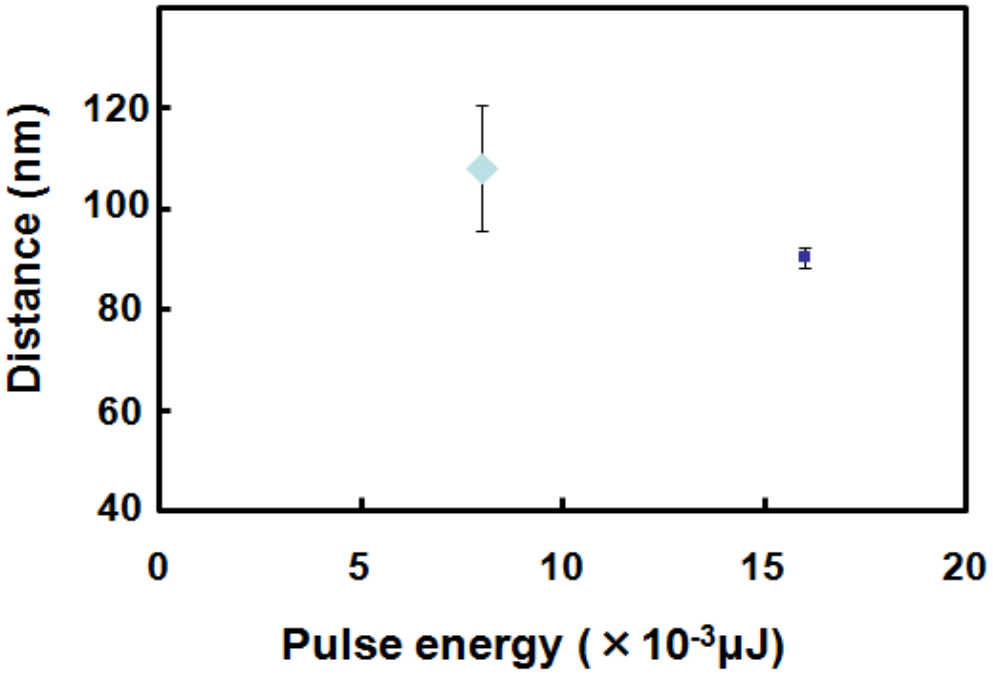

Figure 5. The dependence of the observed periodic nanostructures on the pulse energy under a fixed laser pulses number.

The free electrons are predominantly produced in the Ti thin layer to induce a large change in ε_1. For simplicity, we assume that the film surface before ablation consists of two layers of the upper Ti and the lower Si, as illustrated in the inset of Figure 6. When the surface is weakly corrugated through laser ablation, the surface Plasmon polarizations can be excited at the interfaces between the Ti and Si. The dispersion relation k_{sp} satisfied for the surface Plasmon polarizations excitation was given by

$$\boldsymbol{k_{sp} = k_0 \left[\frac{\varepsilon_a \varepsilon_b}{\varepsilon_a + \varepsilon_b}\right]^{\frac{1}{2}}} \qquad \boldsymbol{(3)}$$

where k_{sp} and k_0 are the wave vectors of the surface plasmon and the incident light in vacuum [22], respectively, and ε_a and ε_b are the relative dielectric constants of two layers concerned. We calculated λ_{sp} for the Ti/Si interface, using $\varepsilon_a = \varepsilon_1 / \varepsilon_0$ for the Ti and $\varepsilon_b = \varepsilon_2 = 13.67 + i \times 0.05$ for the Si [23]. Figure 6 shows the results of λ_{sp} calculated as a function of N_e in the Ti layer. It is noted that the estimated electron density Ne leads to λ_{sp} (176 ~216 nm) for the Ti / Si interface, The local ablation would be initiated at a period d ~ $\lambda_{sp}/2$ with the help of the local field periodically enhanced by the surface Plasmon polarizations. The period d (88~108 nm) calculated for the Ti/Si interface is in almost agreement with the observed size of nanostructure.

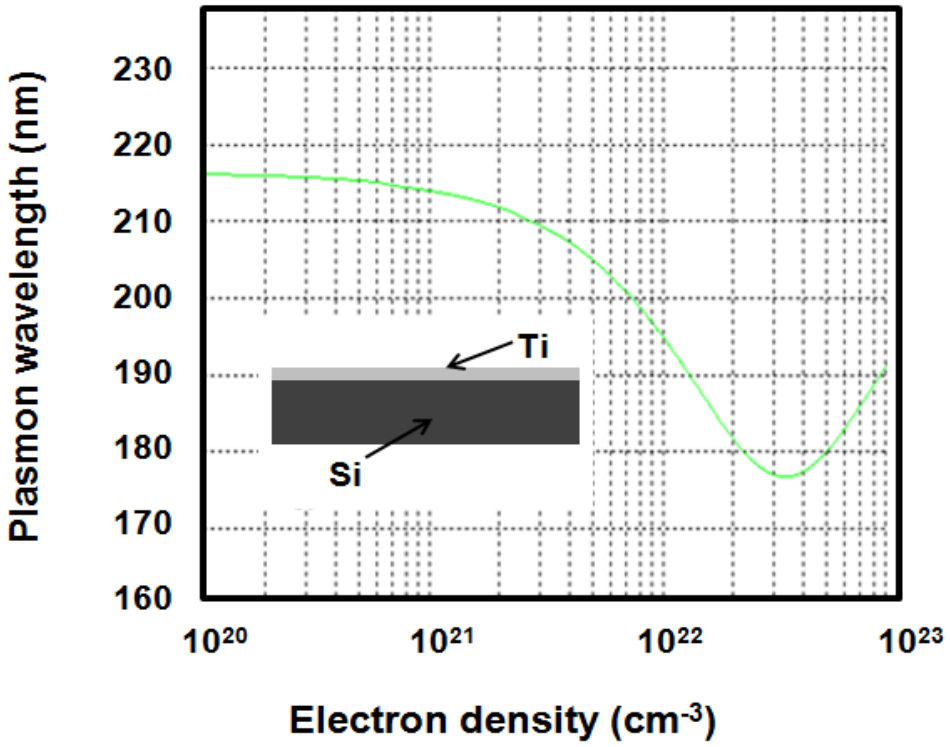

Figure 6. Plasmon wavelength calculated as a function of electron density for the Ti / Si interface.

3.4 Conclusion

In conclusion, periodic nanostructures were controlled fabricated on the Ti thin film surface after irradiation. It was also found that, on the ablated Ti thin film surfaces, the linearly polarized femtosecond laser pulses produce arrays of ripple-like periodic nanostructures which are oriented to the direction parallel to the laser polarization, and a net-like nanostructure was fabricated on the surface of Ti thin film by a technique of two linearly polarized femtosecond laser beams with orthogonal polarizations ablating material alternately. And then the period of self-organized ripple-like nanostructures would be controlled by the pulse energy and the number of irradiated pulses. The estimated field period was almost in agreement with the observed size of nanostructures.

References

[1] C. Spielmann, N. Burnett, S. Sartania, R. Koppitsch, M. Schnurer, C. Kan, M. Lenzner, P. Wobrauschek and F. Krausz, Science **278** (1997) 661.

[2] Z. Chang, A. Rundquist, H. Wang, M. Murnane and H. Kapteyn, Phys. Rev. Lett. **79** (1997) 2967.

[3] S. Chen, A. Maksimchuk and D. Umstadter, Nature (London) **396** (1998) 653.

[4] P. Kazansky, H. Inouye, T. Mitsuyu, K. Miura, J. Qiu, K. Hirao and F. Starrost, Phys. Rev. Lett. **82** (1999) 2199.

[5] K. Miura, J. Qiu, H. Inouye, T. Mitsuyu and K. Hirao, Appl. Phys. Lett. **71** (1997) 3329.

[6] E. Glezer and E. Mazur, Appl. Phys. Lett. **71** (1997) 882.

[7] B. Stuart, M. Feit, A. Rubenchik, B. Shore and M. Perry, Phys. Rev. Lett. **74** (1995) 2248.

[8] D. Du, X. Liu, G. Korn, J. Squier and G. Mourou, Appl. Phys. Lett. **64** (1994) 3071.

[9] J. Reif, F. Costache, M. Henyk and S. V. Pandelov, Appl. Surf. Sci. **197** (2002) 891.

[10] R. Wagner, J. Gottmann, A. Horn and E. W. Kreutz, Appl. Surf. Sci. **252** (2006) 8576.

[11] V. Bhardwaj, E. Simova, P. Rajeev, C. Hnatovsky, R. Taylor, D. Rayner and P. Corkum, Phys. Rev. Lett. **96** (2006) 057404.

[12] A. Vorobyev, V. Makin and C. Guo, J. Appl. Phys. **101** (2007) 034903.

[13] J. Wang and C. Guo, Appl. Phys. Lett. **87** (2005) 251914.

[14] A. Vorobyev and C. Guo, Appl. Phys. A: Mater. Sci. Process. **86** (2007) 321.

[15] D. Emmony, R. Howson and L. Willis, Appl. Phys. Lett. **23** (1973) 598.

[16] J. Sipe, J. Young, J. Preston and H. van Driel, Phys. Rev. B **27** (1983) 1141.

[17] A. Bonch-Bruevich, M. Libenson, V. Makin and V. Trubaev, Opt. Eng. (Bellingham) **31**

(1992) 718.

[18] Y. Shimotsuma, P, Kazansky, J. Qiu and K. Hirao, Phys. Rev. Lett. **91** (2003) 247405.

[19] H. Xu, Z. Sheng and J. Zhang, Chin. Phys. Soc. **56** (2007) 968.

[20] C. Shank, R. Yen and C. Hirlimann, Phys. Rev. Lett. **50** (1983) 454.

[21] P. Johnson and R. Christy, Phys. Rew. B **9** (1974) 5056.

[22] H. Raether, Surface Plasmons on Smooth and Rough Surfaces and on Gratings p.5 (Springer-Verlag, Berlin, 1988).

[23] Data from " Handbook of Optical Constant of Solide " by Edward Palik (1985)

Chapter 4

Photo-initiation of ZnO nanorod formation by femtosecond laser irradiation

4.1 Introduction

Zinc oxide (ZnO) nanostructures have attracted immense attention as they offer a wide bandgap and a large exciton binding energy of 3.37 eV and 60 meV, respectively, at room temperature [1] and ultraviolet emission [2-4]. In particular, ZnO 1D nanostructure such as nanowires and nanorods have been successfully synthesized for various applications ranging from nanolaser [4], gas sensor [5], biosensor [6], field-effect transistor [7], solar cell [8] to field emission [9]. A number of physical and chemical synthesis processes have been employed for the growth of ZnO nanostructures. Some of the physical methods include the thermal evaporation and vapor transport approaches [4, 10], metal organic vapor-phase epitaxial growth (MOVPE) [11], molecular beam epitaxy (MBE) [12] and pulsed laser deposition (PLD) [6], which are generally based on catalyzed vapor-liquid-solid growth mechanism [13]. In addition, the simple and low-cost chemical aqueous solution methods with thermal treatment have also been thoroughly studied [14-19]. However, these processes require one or more of the following rigorous conditions; high temperature, low pressure, complex procedures, long growing durations or the need for catalysts, which inadvertently are embedded on the tips of the nanostructures, introducing undesirable impurity. Although recent

techniques for nucleation of organic [20, 21] and inorganic [22-24] materials with an intense femtosecond laser pulses were proposed, the mechanism is not fully understood. Here we present heterogeneous nucleation induced by the femtosecond laser irradiation in zinc ammine complex ($Zn(NH_3)_n^{2+}$) based aqueous solutions at room temperature and pressure. Such photo-initiated nucleation sites are evidently generated in response to an increase in laser irradiation time and pH value, and subsequently grow into nanorods during low temperature thermal treatments, without the need for catalysts.

4.2 Experimental

Aqueous mixture solutions of 0.02 M $ZnCl_2$ and 0.032 ~ 0.200 M NH_4OH at pH value ranging from 8.5 to 10.5 alkaline environments were initially prepared. We used femtosecond laser pulses to focus a liquid cell and efficiently transfer energy into the precursor solution. The initial solution exhibits a slightly white turbidity decreasing with a pH increase because the formation of zinc ammonia complex, which was subjected to femtosecond pulse irradiation at room temperature.

The laser radiation in Gaussian mode produced by a regenerative amplified mode-locked Ti: sapphire laser (Cyber laser Inc., 230 fs pulse duration, 1kHz repetition rate, pulse energy 0.5 mJ/pulse) operating at a wavelength of 780 nm was focused via 20 × (numerical aperture = 0.45) objective into a rectangular quartz vessel of 1 × 1 × 3.5 cm^3 filled with the precursor solution, which was placed on a magnetic stirrer and continuously stirred to maintain homogeneity. Irradiation was performed for 60 min and the solution subsequently transferred into furnace for heat treatments at 80 ℃ and 100 ℃ for 120 minutes before being cooled down to room temperature. Samples were prepared by drop-casting the solutions onto silicon substrates and allowed to evaporate at room temperature, as illustrated in Figure 1.

The grown ZnO particles were analyzed by field emission scanning electron microscopy (JEOL JSM-6705F) to study their morphologies. X-ray diffraction (XRD) pattern was collected using Rigaku Rint2500HF to study the crystal structure. And room temperature photoluminescence spectrum was obtained via aHoriba Jobin Yvon

FluoroMax-P spectrometer with a Xenon lamp excitation source.

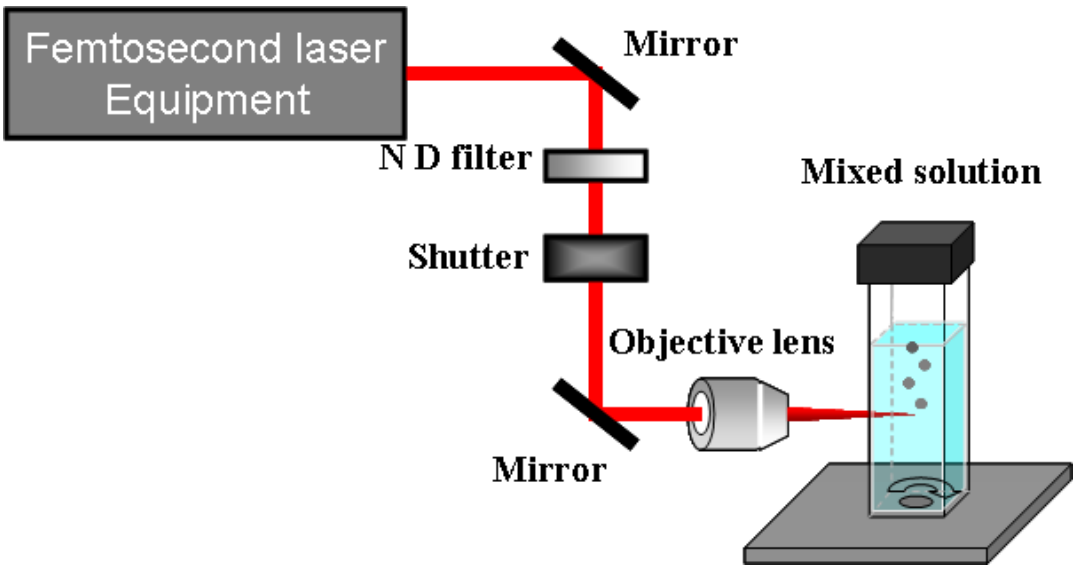

Figure 1. Experimental procedures

4.3 Results and Discussion

The solid phase stability of $Zn(OH)_2$ in the precursor solution was determined by the pH value and the concentration of the Zn(II) soluble species [25]. Figure 2 shows the phase stability diagrams for the $Zn(OH)_2$−NH_3 systems at 25 ℃. The dashed lines indicate the thermodynamic equilibrium between the various Zn(II) soluble species, which are calculated by the following equilibrium equations (1)–(3).

$$Zn^{2+} + iNH_3 \leftrightarrow Zn(NH_3)_i^{2+} \quad (1)$$

$$Zn(NH_3)_i^{2+} + 2OH^- \leftrightarrow Zn(OH)_2\,(s) + iNH_3 \quad (2)$$

$$Zn(OH)_2\,(s) \leftrightarrow Zn(OH)_2\,(aq.) \quad (3)$$

Values of standard thermodynamic data and stability constant are taken from the literature [25-28]. The red solid line represents the boundary of the solubility of the solid $Zn(OH)_2$. This diagram reveals that the solid $Zn(OH)_2$ is thermodynamically stable at a pH value ranging from 7 to 12 in a precursor solution containing a Zn concentration of 0.02 M. Typical three precursor solutions with different pH values of 8.5, 9.5, and 10.5 were prepared in the present study.

No apparent diffraction peaks of ZnO were observed in the case of the thermal precipitates from precursor solutions at every pH condition without the laser irradiation (Figure 3(a)). These patterns were assigned to $Zn(OH)_2$ and $Zn_5(OH)_8Cl_2.H_2O$, suggesting that the precursor solutions could not become supersaturated at low temperature of 80 ℃ with respect to the homogeneous ZnO nucleation.

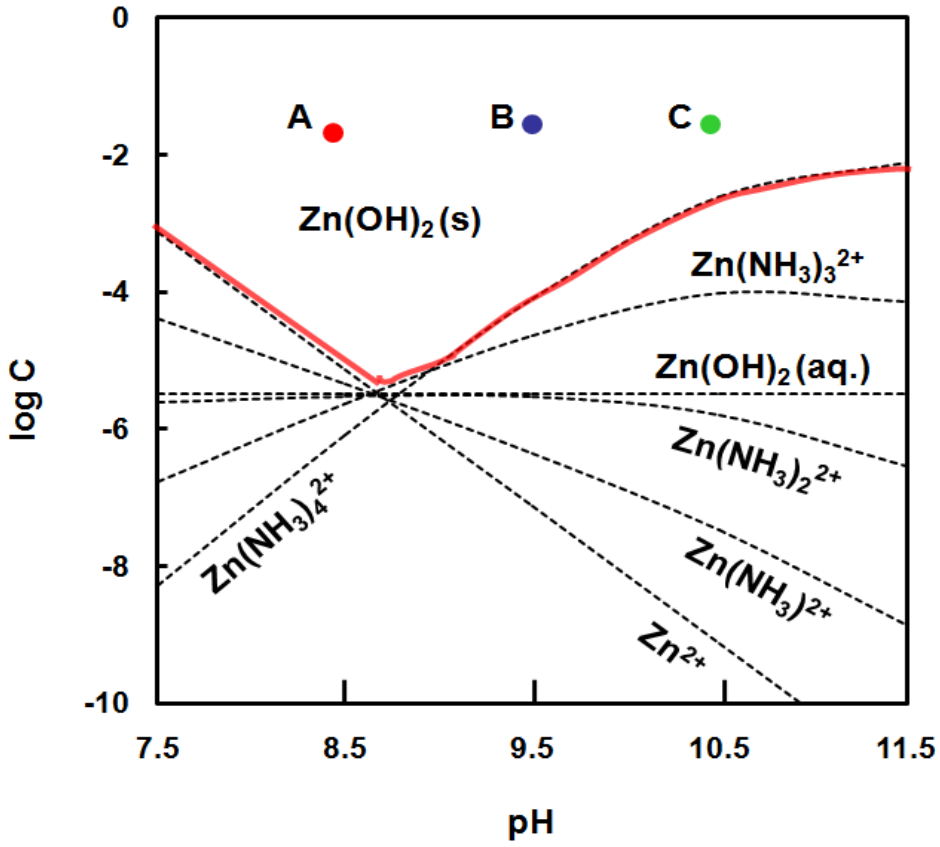

Figure 2. Phase stability diagram for $Zn(OH)_2$–NH_3 system at 25 ℃ as a function of pH. The points marked by A, B, and C represent the preparation conditions of precursor solution in this study. The dashed lines indicate the thermodynamic equilibrium between the various Zn(II) soluble species and the solid $Zn(OH)_2$. The red solid line represents the boundary of the solubility of the solid $Zn(OH)_2$.

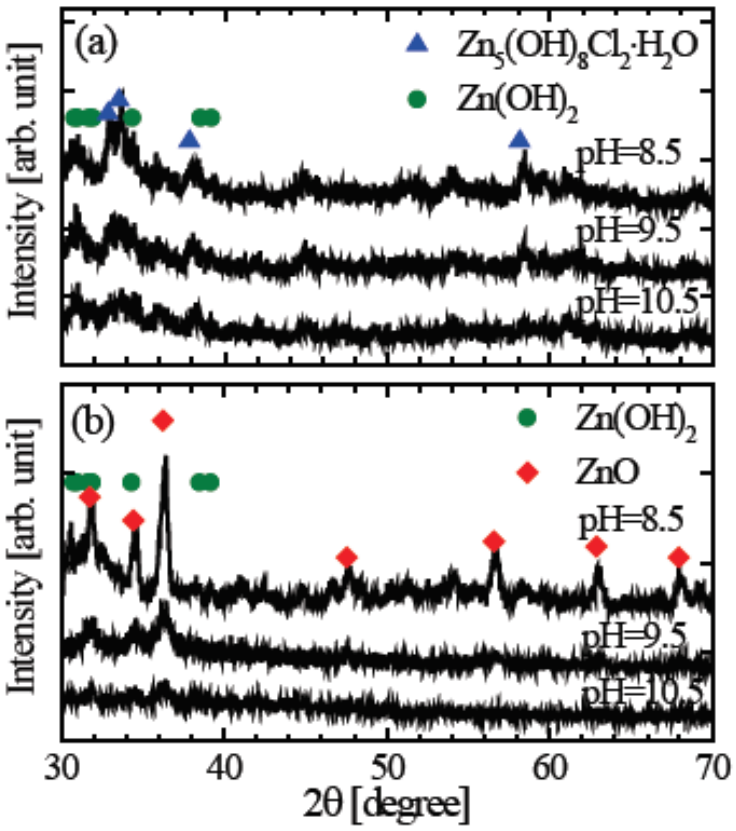

Figure 3. XRD patterns of precipitates from mixed precursor solutions at pH 8.5, 9.5, and 10.5 without (a) and with (b) the femtosecond laser irradiation for 60 minutes and the successive thermal treatment at 80 ℃ for 120 minutes. The JCPDS standards of $Zn_5(OH)_8Cl_2$. H_2O (▲), $Zn(OH)_2$ (●), and ZnO (■) are also shown.

On the other hand, the apparent diffraction peaks attributed to ZnO were observed by applying laser irradiation process before thermal treatment at the same temperature (Figure 3(b)). This indicates that the photo-initiated heterogeneous nucleation induced by the femtosecond laser irradiation could occur in precursor solution at room temperature. The SEM images in Figure 4 evidently indicate that in contrast to the formation of the amorphous precipitate during the thermal treatment at 80 ℃ for 120 minutes, the ZnO hexagonal nanorods with a diameter of 40 ~ 80nm, which slightly decreases with pH value increasing, were obtained by applying the laser irradiation (Figure 4(d)-(f)).

Based on these results, photo-initiated nucleation process resulting from local supersaturation at room temperature via femtosecond laser pulse irradiation could be proposed In order to reveal the nucleation and growth mechanisms of ZnO nanorods with the additional femtosecond laser irradiation process, the heating temperature during the successive thermal treatment was changed up to 100 ℃.

ZnO nanoparticles were precipitated with or without laser irradiation (Figure 5). The shape of ZnO nanoparticles was changed from nanorods to flower-like with increasing the pH in the thermal treatment (Figure 5(a), (c)). In addition, the smaller ZnO nanoparticles resulting from secondary nucleation were observed at the pH of 9.5 (Figure 5(b)).

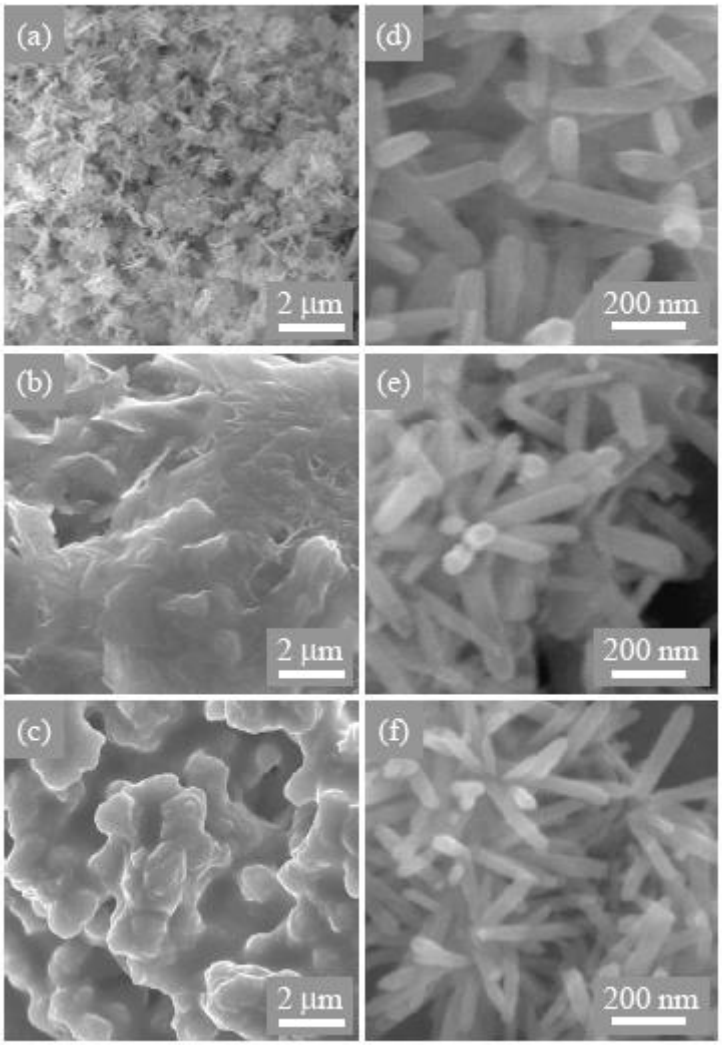

Figure 4. SEM micrographs of precipitates synthesized from mixed precursor solutions at pH 8.5 (a, d), 9.5 (b, e), and 10.5 (c, f) by the thermal treatment at 80 ℃ for 120 minutes (left column) and the additional laser irradiation before the thermal treatment (right column).

It is well known that the flower-like ZnO nanostructures are formed via twinned ZnO nuclei along the (11-22) planes in the system with higher supersaturation of $Zn(OH)_4^{2-}$ [29]. On the other hand, ultrafine ZnO nanorods with a diameter of 20 ~ 70 nm were formed by the additional laser irradiation compared to that of the thermal process regardless of pH, about 4 times thinner nanorods were especially formed at the pH of 8.5 (Figure 5(a), (d)). The size of ZnO nanorods obtained by the laser irradiation increased with an increase in pH (Figure 5(d)-(f)).

Comparison of the effect of temperature on the size of ZnO nanorods between 80 ℃ and 100 ℃ with the laser irradiation indicates that the size decreases with increasing temperature from pH 8.5 to 9.5, although the size increases with increasing temperature at pH of 10.5 (Figure 4(d)-(f), Figure 5(d)-(f)).

Based on the difference in the shape and size of ZnO nanostructures with and without the femtosecond laser irradiation before the subsequent thermal treatment, we deduce the formation mechanism of ZnO nanorods below. The possible reactions in our experiments can be summarized in the following equations (4)–(7).

$$Zn^{2+} + 2OH^- \leftrightarrow Zn(OH)_2\ (s) \quad (4)$$

$$Zn(OH)_2\ (s) \rightarrow ZnO + H_2O \quad (5)$$

$$Zn^{2+} + 4NH_3 \leftrightarrow Zn(NH_3)_i^{2+} \quad (6)$$

$$Zn(NH_3)_4^{2+} + 2OH^- \rightarrow ZnO + 4NH_3 + H_2O \quad (7)$$

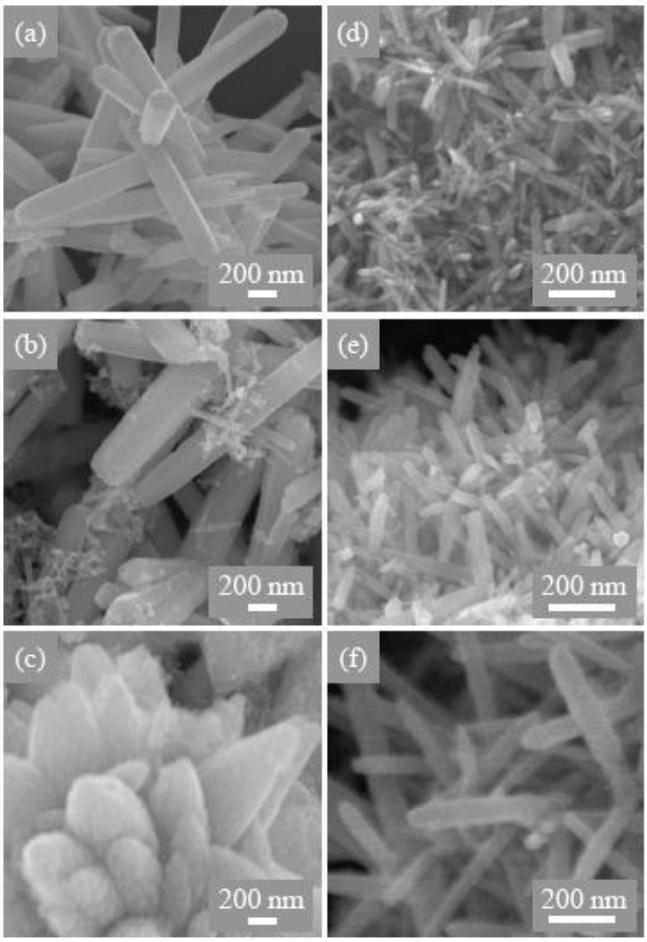

Figure 5. SEM micrographs of precipitates synthesized from mixed precursor solutions at pH 8.5 (a, d), 9.5 (b, e), and 10.5 (c, f) by the thermal treatment at 100 ℃ for 120 minutes (left column) and the additional laser irradiation before the thermal treatment (right column).

In the experimental pH region, we could consider the soluble species of the uncomplexed Zn^{2+} ions and the zinc-ammonia complex ions of $Zn(NH_3)_4^{2+}$ at a much higher concentration of NH_3. In addition, the insoluble compounds of $Zn(OH)_2$ can be formed in this system. The calculated concentration of $Zn(NH_3)_4^{2+}$ and solid $Zn(OH)_2$ in mixed precursor solutions are shown in Table 1.

The size of obtained ZnO nanorods produced by the femtosecond laser irradiation at 0.5 mJ for 60 minutes and the successive thermal treatment at 100 ℃ for 120 minutes are also shown. The amount of such precipitation depends on the pH and the concentration of NH_3 in the solution based on the solubility of $Zn(OH)_2$ and the dissociation constants of $Zn(NH_3)_4^{2+}$. At the pH of 8.5 and 9.5, the reaction of Eq. (4) is dominant and the equilibrium moves to right, namely the nuclei of ZnO are predominantly formed from $Zn(OH)_2$ by the laser irradiation. In contrast, a large amount of the soluble complexes ions of $Zn(NH_3)_4^{2+}$ in addition to the precipitation could be consumed by the formation of ZnO nuclei during laser irradiation, because the reaction of Eq. (6) is dominant at the pH of 10.5. Indeed, the energy absorption by the focusing of femtosecond laser pulses was almost same of 66 % regardless of the pH, although the scattered light intensities at the pH of 8.5 and 9.5 was about 2.5 times higher than that at the pH of 10.5. During the subsequent thermal treatment after the laser irradiation, ZnO nuclei formed by the different reaction path grow into ZnO nanorods along the c-axis direction [30].

Table 1. Calculated concentration of soluble and insoluble Zn(II) species and the corresponding the size of obtained ZnO nanorods[a]

pH	$Zn(NH_3)_4^{2+}$ [mol/L]	$Zn(OH)_2(s)$ [mol/L]	ZnO nanorods	
			Diameter (nm)	Length (nm)
8.5	8.1×10^{-7}	9.1×10^{-3}	38(±7)	168(±5)
9.5	7.8×10^{-5}	9.1×10^{-3}	44(±5)	233(±3)
10.5	2.4×10^{-3}	6.6×10^{-3}	68(±24)	515(±46)

[a] The ZnO nanorods are formed by the femtosecond laser irradiation at 0.5 μJ for 60 minutes and the successive thermal treatment at 100 ℃ for 120 minutes. The numbers in the parenthesis show the standard deviation for 20 samples.

In lower pH solution (pH 8.5), the smaller ZnO nanorods are formed by the secondary nucleation and growth during the hydrothermal process (Figure 4(d)). On the other hand, the larger nanorods could be obtained because ZnO nuclei formed by the laser irradiation grow dominantly during the thermal treatment. It is noted that the standard Gibbs free energy changes of Eq. (5) and (7) are -3.94 and -47.2 kJ/mol, respectively.

To discuss the dynamics of ZnO nuclei formation during the femtosecond laser irradiation, we measured the evolution of spectral extinction of the precursor solutions during the femtosecond laser irradiation (Figure 6). The transmitted visible light was detected by a photonic multi- channel analyzer (Hamamatsu Photonics, PMA-11). The components of the extinction in Figure 6 include the sum of light scattering and absorption by ZnO nuclei formed by the laser irradiation.

Assuming that the visible absorption of ZnO is negligible, we could estimate the dynamics of the photo-initiated nucleation process based on the Rayleigh scattering theory. In the Rayleigh scattering regime, the scattered light intensity is inversely proportional to the fourth power of wavelength, indicating the shorter wavelength will scatter more than the longer wavelength. While the scattered light intensity in the lower pH solution was substantially constant (Figure 6(a)), in the higher pH solution, the scattered light intensity in the shorter wavelength region increases with an increasing in laser irradiation time (Figure 6(c)). The results clearly indicate that ZnO nuclei are produced from the liquid phase, i.e. Eq. (6) and (7), in the higher pH solution.

On the other hand, the scattering light intensity does not change dramatically because solid $Zn(OH)_2$ already exists in the lower pH solution (Eq. (4) and (5)). Finally, ZnO nuclei produced through different reaction pathways grow into ZnO nanorods during the successive thermal treatment even in the higher pH solution. In order to understanding the origin of the observed phenomenon, the following explanation of the heating mechanism is proposed. Since the light intensity in the focus of the beam is of 10^{16} W/cm^2, the plasma is produced by multiphoton ionization in the focal volume.

Once a high free electron density is produced by multiphoton ionization, the material has the properties of plasma and will absorb the laser energy via absorption mechanism of inverse Bremstrahlung heating. Assuming that the electron temperature is proportional to the pulse energy, the electron temperature can be roughly estimated by a simple formula: $Q = CeVTe$, where $Q (= \eta E)$ is the absorbed energy, $\eta$is the absorption coefficient, E is the pulse energy, V is the volume interaction, Te is the electron temperature, and Ce is the electron heat capacity. Within the free electron gas model, The electron heat capacity can be approximately calculated by $Ce(Te) = \gamma Te$, where $\gamma = \pi^2 n_e \kappa_B^2 / 2I_E$ [31], where ne is the electron number density, κ_B is the Boltzmann constant, I_E is the ionization potential. The electron temperature is estimated to be 1.3 keV ($\sim 1.5\times10^7$ K) by using the parameters in Table 2, which corresponds to the experimental results [32].

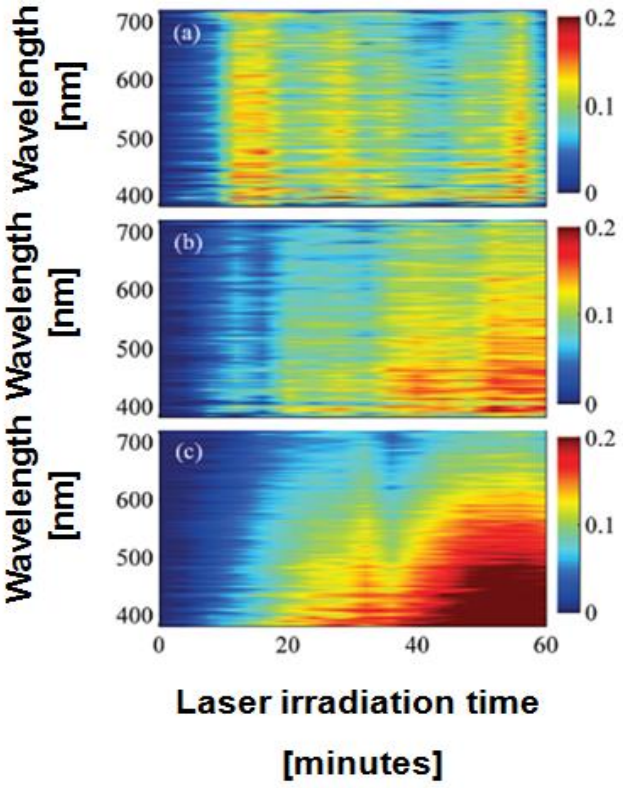

Figure 6. Evolution of visible extinction spectra of the precursor solution at pH 8.5 (a), 9.5 (b), and 10.5 (c) during femtosecond laser irradiation. The components of the extinction include the sum of light scattering and absorption by ZnO nuclei formed by the laser irradiation.

Based on this calculation, not only the optical breakdown, bubble formation, but also the dissociation of the precursor solution could occur within the focal volume during the femtosecond laser irradiation. Such very high electron temperature decreases with an increase of the lattice temperature, then it reaches to the same temperature as lattice temperature with a time scale of several picoseconds. Assuming that the initial temperature of focal volume reaches ΔT_0 = 3000K after the electron-phonon coupling, the thermal diffusivity can be calculated by the following equation.

For simplicity, we used the thermal diffusivity coefficient of distill water (Dth = 1.43×107 m2/s)

$$\Delta T(r,t) = \Delta T_0 \left(\frac{w_0}{\sqrt{{w_0}^2 + 4D_{th}t}} \right)^3 \exp\left(-\frac{r^2}{w_0^2 + 4D_{th}t} \right) \quad (8)$$

Where T_0 is the initial temperature just after the femtosecond single pulse irradiation, w_0 is the laser beam waist, t is the time after the irradiation, and r is the distance from the focus. Figure 7 indicates the calculated temperature distributions just after the femtosecond single pulse irradiation as a function of the distance from focus. In this calculation, the time after the laser irradiation were changed from 0 s to 100 μs. Since the repetition rate of 1 kHz, i.e. the interpulse time of 1 ms in the experiments, these calculations apparently indicate that the heat induced by the first pulse can diffuse away from the focal region before the arrival of the successive pulse.

Table 2. Parameter for the Calculation of the Electron Themperature

Material	Water	-
Density, ρ	1.0×10^{3}	[kg/m^3]
Molar weight, M	1.8×10^{-2}	[kg/mol]
Ionization potensial, I_E	6.5	[ev]
Laser wavelength, λ	7.8×10^{-7}	[m]
Pulse-width, τ_p	2.3×10^{-13}	[s]
Pulse energy, E	5.0×10^{-4}	[J]
Absorption coefficient, η	0.2	-
Electron density, n_e	1.0×10^{20}	[cm^{-3}]
Numerical aperture, NA	0.45	-

Indeed, no apparent temperature change occurred after the femtosecond laser irradiation for 60min. The ZnO nucleation induced by the femtosecond laser irradiation could occur at the instantaneous high-temperature region surrounding the focal volume in precursor solution at room temperature.

Based on the experimental results, the possible formation mechanism of the ZnO nanorods was proposed. Upon mixing the starting reagent, the soluble complexation species of $Zn(NH_3)_4^{2+}$ [33-35] were formed in alkaline environment. Nucleus is then produced in the solutions via hexagonal nucleation by laser irradiation. Acting as the growth units, $Zn(NH_3)_4^{2+}$ were then dehydrated to ZnO at elevated temperatures to construct the ZnO nanostructures, as illustrated in figure 8.

One-dimensional growth of ZnO crystal structure is that O-Zn-O-Zn-O layered in C-axis direction. In addition, the tail end is oxygen layer. The precursor $Zn(NH_3)_4^{2+}$ interacts with the oxygen on tail end layer by coulomb attraction, the growth speed in C-axis direction get faster than the growth speed in the other directions, leading to the growth of rod-like ZnO nanostructure, as illustrated in figure 9.

Figure 10 shows the room temperature photoluminescence of ZnO nanorods, with a UV emission peaking at ~380 nm that is ascribed to the ZnO band-edge emission due to the recombination of free excitons [36-39]. The broad green emission observed beyond ~530 nm is generally accepted as deep-level or trap-state emission due to irradiative recombination of a photogenerated hole with an electron occupying the oxygen vacancy [40-43].

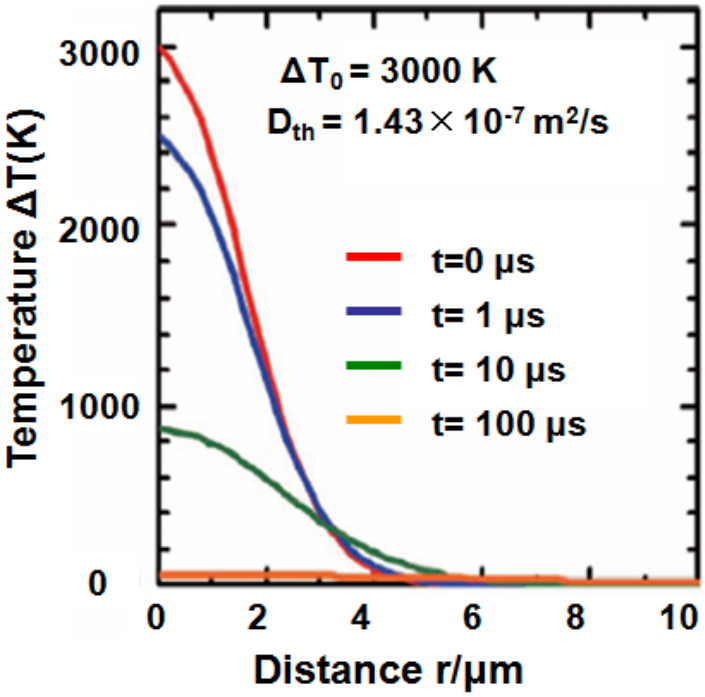

Figure 7. Calculated temperature distributions just after the femtosecond single pulse irradiation as a function of the distance from focus. In this calculation, the time after the laser irradiation were changed from 0 μs to 100 μs.

The broad spectrum and low intensity observed could be due to poor ZnO crystal quality caused by OH^- attack, the low intensity Xenon lamp source used or the random alignment of the nanorods, resulting in poor luminescence. In addition, coatings of organic solutions could be present on the nanorod surfaces, affecting the results and possibly giving rise to the peaks seen at ~450–470 nm.

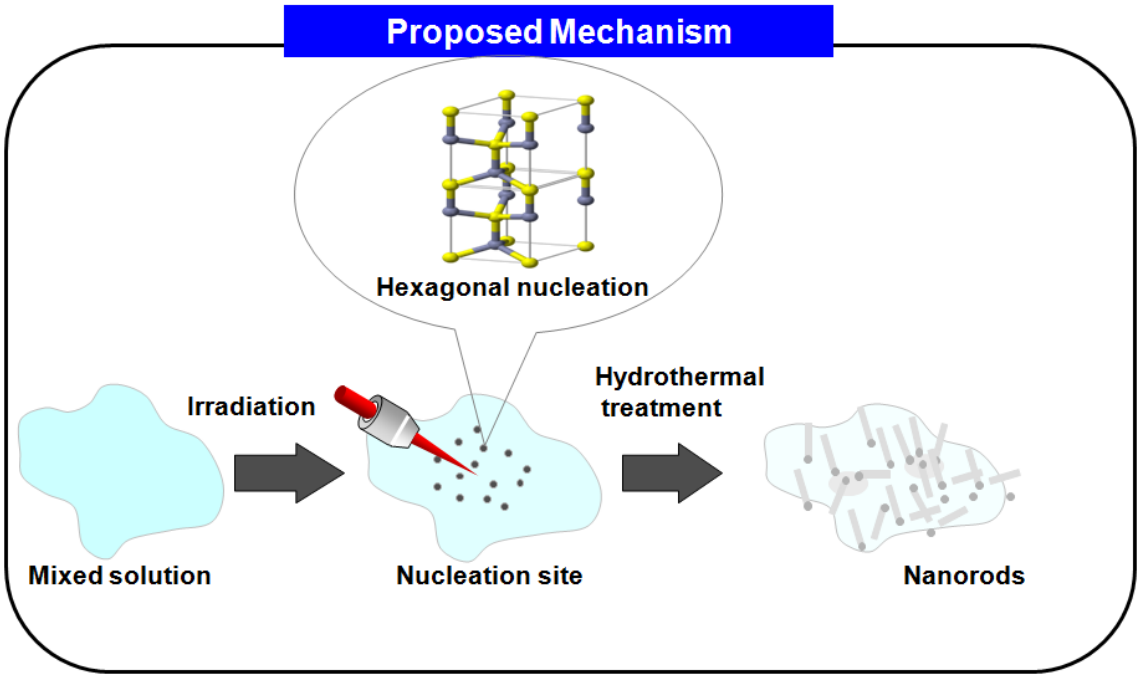

Figure 8. Schematic illustration of the proposed mechanism of ZnO nanorods formation by femtosecond laser irradiation.

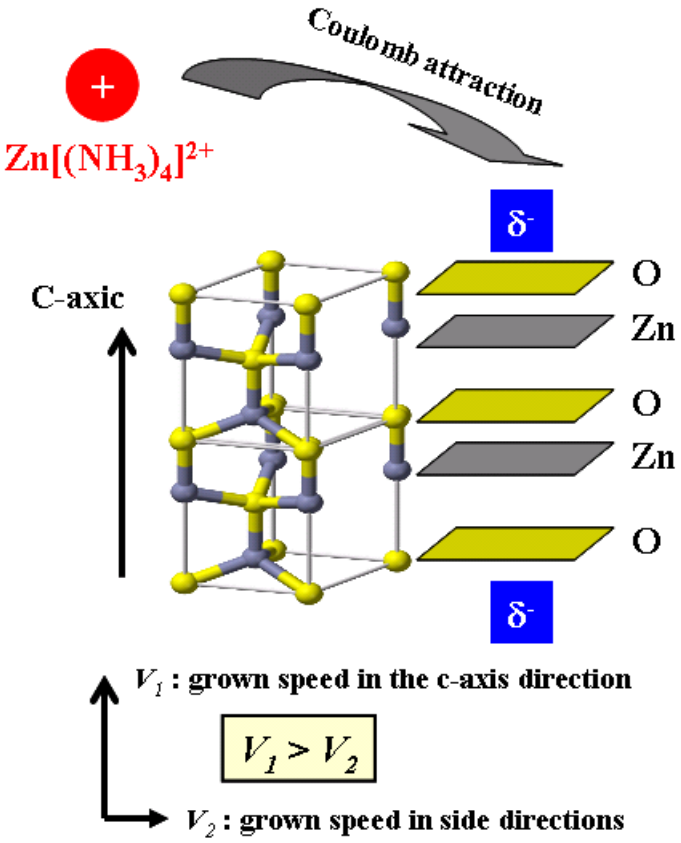

Figure 9. Schematic representation of one-dimensional ZnO nanorods growth.

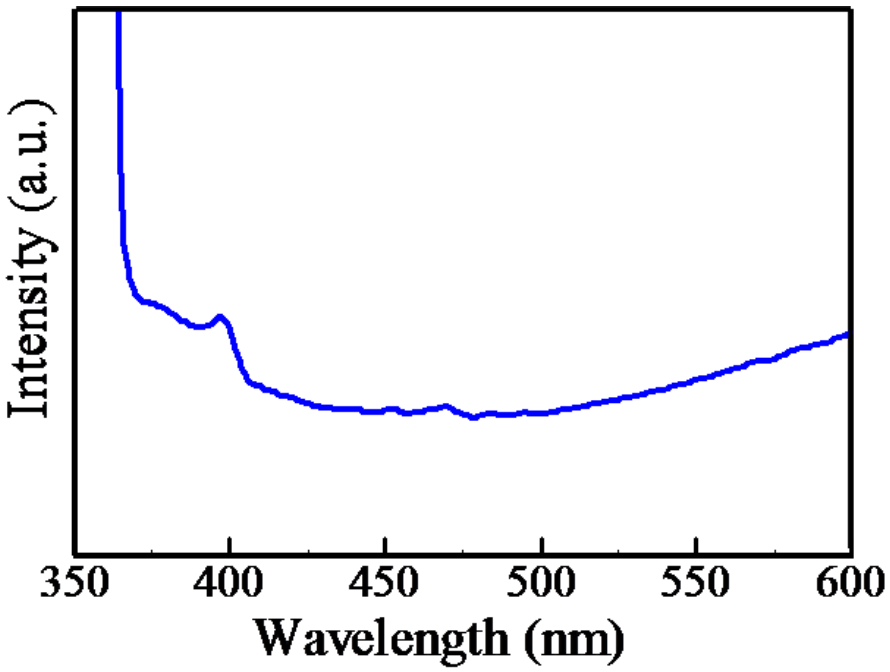

Figure 10. photoluminescence of ZnO nanorods at pH 9.5 with the femtosecond laser irradiation for 60 minutes and the thermal successive treatment at 100 ^{o}C for 120 minutes.

4.4 Conclusions

In conclusion, ZnO nanorods have been successfully synthesized from heterogeneous nucleation initiated by femtosecond laser irradiation in aqueous solutions with subsequent hydrothermal treatments. Due to the localized high supersaturation of precursor solution, the size of the obtained hexagonal ZnO nanorods with femtosecond laser irradiation and the subsequent thermal treatment is about 4 times thinner than that obtained by the thermal treatment. Studies involving pH variation indicate that ZnO nucleus produced through different reaction pathways according to the pH value of the precursor solution. The size of the obtained hexagonal ZnO nanorods is variable according to the pH of the precursor solution. Apart from the fundamental importance of the mechanism of ZnO nucleation, the photo-initiated ZnO nucleation via femtosecond laser irradiation could be useful for chemical reaction in liquid phase.

References

[1] H. Ohta and H. Hosono, Mater. Today **7** (2004) 42.

[2] P.-F. Lin, C.-Y. Ko, W.-T. Lin and C.T. Lee, Mater. Lett. **61** (2007) 1767.

[3] Y. C. Kong, D. P. Yu, B. Zhang, W. Fang and S. Q. Feng, Appl. Phys. Lett. **78** (2001) 407.

[4] M. H. Huang, S. Mao, H. Feick, H. Yan, Y. Wu, H. Kind, E. Weber, R. Russo and P. Yang, Science **292** (2001) 1897.

[5] G. Sberveglieri, C. Baratto, E. Comini, G. Faglia, M. Ferroni, A. Ponzoni and A. Vomiero, Sens. Actuators B **121** (2007) 208.

[6] F. Zhang, X. Wang, S. Ai, Z. Sun, Q. Wan, Z. Zhu, Y. Xian, L. Jin and K. Yamamoto, Anal. Chim. Acta. **519** (2004) 155.

[7] M. S. Arnold, P. Avouris, Z. W. Pan and Z. L. Wang, J. Phys. Chem. B **107** (2003) 659.

[8] E. Hosono, S. Fujihara, I. Honma and H. Zhou, Adv. Mater. **17** (2005) 2091.

[9] C. J. Lee, T. J. Lee, S. C. Lyu, Y. Zhang, H. Ruh and H. J. Lee, Appl. Phys. Lett. **81** (2002) 3648.

[10] Z. W. Pan, Z. R. Dai and Z. L. Wang, Science **292** (2001) 1897.

[11] W. I. Park, D. H. Kim, S.-W. Jung and G.-C. Yi, Appl. Phys. Lett. **80** (2002) 4232.

[12] Y. W. Heo, V. Varadarajan, M. Kaufman, K. Kim, D. P. Norton, F. Ren and P. H. Fleming, Appl. Phys. Lett. **81** (2002) 3046.

[13] R. S. Wagner and W. C. Ellis, Appl. Phys. Lett. **4** (1964) 89.

[14] J. Zhang, L. Sun, C. Liao and C. Yan, Chem. Commun. **3** (2002) 262.

[15] X. Y. Zhang, J. Y. Dai, H. C. Ong, N. Wang, H. L. W. Chan and C. L. Cho, Chem. Phys. Lett. **393** (2004) 17.

[16] H. Q. Le, S. J. Chua, Y. W. Koh, K. P. Loh, Z. Chen, C. V. Thompson and E. A. Fitzgerald, Appl. Phys. Lett. **87** (2005) 101908.

[17] H. Zhang, D. Yang, X. Ma, Y. Ji, J. Xu and D. Que, Nanotechnology **15** (2004) 622.

[18] M. Yang, G. Pang, L. Jiang and S. Feng, Nanotechnology **17** (2006) 206.

[19] J. Zhang, L. D. Sun, J. L. Yin, H. L. Su, C. S. Liao and C. H. Yan: Chem. Mater. **14** (2002) 4172.

[20] H. Adachi, K. Takano, Y. Hosokawa, T. Inoue, Y. Mori, H. Matsumura, M. Yoshimura, Y. Tsunaka, M. Morikawa, S. Kanaya, H. Masuhara, Y. Kai and T. Sasak, Jpn. J. Appl. Phys. **42** (2003) L798.

[21] H. Y. Yoshikawa, R. Murai, S. Maki, T. Kitatani, S. Sugiyama, G. Sazaki, H. Adachi, T. Inoue, H. TMatsumura, K. akano, S. Murakami, T. Sasaki and Y. Mori, Appl. Phys. A **93** (2008) 911.

[22] Y. Shimotsuma, T. Yuasa, H. Homma, M. Sakakura, A. Nakao, K. Miura, K. Hirao, M. Kawasaki, J. Qiu and P. G. Kazansky, Chem. Mater. **19** (2007) 1206.

[23] E. T. Y. Lee, Y. Shimotsuma, M. Sakakura, M. Nishi, K. Miura and K. Hirao, Mater. Lett. **62** (2008) 4044.

[24] E. T. Y. Lee, Y. Shimotsuma, M. Sakakura, M. Nishi, K. Miura and K. Hirao, J. Nanosci. Nanotechnol. **9** (2009) 618.

[25] S. Yamabi and H. J. Imai, Mater. Chem. **12** (2002) 3773.

[26] S. Peulon and D. J. Lincot, Electrochem. Soc. **145** (1998) 864.

[27] A. Goux, T. Pauporté , J. Chivot and D. Lincot, Electrochim. Acta **50** (2005) 2239.

[28] B. Hubert, N. Naghavi, B. Canava, A. Etcheberry and D. Lincot, Thin Solid Films **515** (2007) 6032.

[29] Y. Zhang and J. Mu, Nanotechnology 18 (2007) 075606.

[30] S. Baruah and J. Dutta, Sci. Technol. Adv. Mater. **10** (2009) 013001.

[31] Z. Lin, L. V. Zhigilei and V. Celli, Phys. Rev. B, **77** (2008) 1.

[32] K. Hatanaka, T. Miura and H. Fukumura, Chem. Phys. **299** (2004) 265.

[33] W. Li, E. Shi, W. Zhong and Z. J. Yin, J. Cryst. Growth. **203** (1999) 186

[34] R. Fratesi and G. Roventi, J. Appl. Electrochem. **22** (1992) 657.

[35] E. T. Y. Lee, Y. Shimotsuma, M. Sakakura, M. Nishi, K. Miura and K. Hirao Materials letters **62** (2008) 4044.

[36] M. H. Huang, Y. Y. Wu, H. N. Feick, N. Tran, E. Weber and P. D. Yang, Adv. Mater. **13** (2001) 175.

[37] J. Zhang, L. Sun, J. Yin, H. Su, C. Liao and C. Yan. Chem. Mater. **14** (2002) 4172.

[38] M.H. Huang, Y.Y. Wu, H.N. Feick, N. Tran, E. Weber and P.D. Yang. Adv. Mater. **13** (2001) 113.

[39] S. Monticone and R. Tufeu. A.V. Kanaev. J. Phys. Chem. B, **102** (1998) 2853.

[40] K. Vanheusden, W. L. Warren, C. H. Seager, D. R. Tallant, J. A. Voigt and B. E. Gnade, J. Appl. Phys. **176** (1996) 7983.

[41] K. Hoffmann and D. Hahn, Phys. Status Solidi A. 24 (1974) 637.

[42] A. Po¨ppl and G. Vo¨lkel, Phys. Status Solidi A. 121 (1990) 195.

[43] K. Vanheusden, W. L. Warren, J. A. Voigt, C. H. Seager, and D. R. Tallant, Appl. Phys. Lett. 67 (1995) 1280

Summary

The ultrafast laser is a powerful tool to clarity elementary processes, such as excitation-energy relaxation and both electron and proton transfer on nanosecond and picoseconds time scales that occur in a micrometer-sized area. Due to the ultrashort light-matter interaction time and the high peak power density, material processing with the femtosecond laser is generally characterized by the absence of heat diffusion and consequently molted layers. The photo-induced reactions are expected to occur only near the focused part of the laser beam due to multiphoton processes. Therefore, much attention has been paid to manufacture micromachine by using femtosecond laser irradiation.

In this present thesis, femtosecond laser has been utilized for micro-structure of different materials. First, a new method had been developed that can selectively plate with drawing directly on the surface of Ag_2O-doped glass using a femtosecond laser. It means that the copper can be plated selectively. Then, a study of nano-structrues of various periodic on the film surface was investigated. One-dimensional periodic structure as nano-ripple or nano-grating had been formed. Also, not just one-dimension, a two-dimensional nanostructure as nano-net was also produced by femtosecond laser irradiation. Furthermore, not just investigate light-matter interaction of the solid, my studies are also expanded to light- liquid interaction, and the synthesis of ZnO nanorods can be controlled in aqueous solution. The results obtained are summarized as follows.

In Chapter 1: The concept of femtosecond laser, a new regime of light – matter

interactions are reviewed. The current state and future perspective of the femtosecond laser applications and efforts in the development of new materials are described.

In Chapter 2: A new method had been investigated that the selective metallization can be carried out on Ag_2O-doped silicate glass under femtosecond laser irradiation after electroless plating. Due to the multiphoton reduction process, the reduction of an Ag ion to an atom by Femtosecond Laser irradiation is essential in forming Ag nanoparticles, and the Ag atom acts as a crystal nucleus for copper growth. The copper thin film can be deposited only on the irradiation regions, when electroless Cu plating process is performed. The results were obtained that the line widths of the ablated region and the plated Cu increase from 2.5 to 7.5 μm and from 7.4 to 25.4 μm, the groove depths of the ablated region increase from 4.8 to 29 μm, respectively, as the laser power increases.

In Chapter 3: In conclusion, periodic nanostructures were controlled to fabricate on the Ti thin film surface after irradiation. The results were obtained that, on the ablated Ti thin film surfaces, the linearly polarized femtosecond laser pulses produce arrays of ripple-like periodic nanostructures which are oriented to the direction parallel to the laser polarization, and a net-like nanostructure was fabricated on the surface of Ti thin film by a technique of two linearly polarized femtosecond laser beams with orthogonal polarizations ablating material alternately. And then the period of self-organized ripple-like nanostructures would be controlled by the pulse energy and the number of irradiated pulses. The estimated field period was almost in agreement with the observed size of nanostructures.

In Chapter 4: In this chapter, ZnO nanorods have been successfully synthesized from heterogeneous nucleation initiated by femtosecond laser irradiation in aqueous solutions

with subsequent hydrothermal treatments. Due to the localized high supersaturation of precursor solution, the size of the obtained hexagonal ZnO nanorods with femtosecond laser irradiation and the subsequent thermal treatment is about 4 times thinner than that obtained by the thermal treatment. Studies involving pH variation indicate that ZnO nucleus produced through different reaction pathways according to the pH value of the precursor solution.

List of Publications

Chapter 1

"Space selective reduction of europium ions via SrF_2 crystals induced by high repetition rate femtosecond laser"

Xi Wang, Nan Wu, Masahiro Shimizu, Masaaki Sakakura, Yasuhiko Shimotsuma, Kiyotaka Miura, Shifeng Zhou, Jianrong Qiu and Kazuyuki Hirao

Journal of the Ceramic Society of Japan 119 [12] 939-941, 2011

Chapter 2

"Selective metallization of Ag_2O-doped silicate glass by femtosecond laser direct writing"

Nan Wu, Xi Wang, Zhenxuan Wang, Masatoshi Ohnishi, Masayuki Nishi, Kiyotaka Miura and Kazuyuki Hirao

Journal of the Ceramic Society of Japan 119 [9] 697-700, 2011

Chapter 3

"Nano-periodic structure formation on titanium thin film with a Femtosecond laser"

Nan Wu, Zhenxuan Wang, Xi Wang, Yasuhiko Shimotsuma, Masayuki Nishi, Kiyotaka Miura and Kazuyuki Hirao

Journal of the Ceramic Society of Japan 119 [11] 898-901, 2011

“Studies on nano-periodic structure formation on the surface of titanium thin film with a femtosecond laser”

Nan Wu, Zhenxuan Wang, Xi Wang, Yasuhiko Shimotsuma, Masayuki Nishi, Kiyotaka Miura and Kazuyuki Hirao

Journal of Applied Physics, in press

Chapter 4

“Photo-initiation of ZnO nanowire formation by femtosecond laser irradiation”

Nan Wu, Yasuhiko Shimotsuma, Masaaki Sakakura, Masayuki Nishi, Kiyotaka Miura and Kazuyuki Hirao

Journal of the Ceramic Society of Japan 118[2] 147-151, 2010

“Studies on photo-initiation of ZnO nano-structure by femtosecond laser irradiation”

Nan Wu, Yasuhiko Shimotsuma, Masaaki Sakakura, Masayuki Nishi, Kiyotaka Miura and Kazuyuki Hirao

Journal of Optics Letters, submitted

Acknowledgements

The present thesis has been carried out at Graduate School of Engineering, Kyoto University under the supervision of Professor Kazuyuki Hirao.

The author wishes to express his sincere gratitude to Prof. Hirao, who granted me the chance to study in Kyoto University. Their wise guide and valuable suggestions enlightened me throughout the whole period of doctor course study.

I am also deeply indebted to, Prof. Kiyotaka Miura and Dr. Yasuhiko Shimotsuma, Dr. Masaaki Sakakura, Dr. Masayuki Nishi, Shingo Kanehira, and Mr. Masatoshi Ohnishi. Their great help and instructive discussion made me thoroughly understand the function of the equipments during the experiments as well as the mechanism of femtosecond laser processing.

Heartily thanks to Dr. Zhenxuan Wang, Dr. Shifeng Zhou for their helpful support and profitable suggestions.

Grateful acknowledgment is made to Mr. Xi Wang and Miss Miki Tahara, who has given me a lot of advice about the experiments and life in Japan.

Finally, the author is deeply grateful to his parents for their understanding, supports, and encouragements.

Kyoto University, 2012

Nan Wu